Doctoral Dissertation

Synthesis of nanomaterials by the impulse plasma in liquid

March 2008

Emil Omurzak

Graduate School of Science and Technology

KUMAMOTO UNIVERSITY

CONTENTS

Title: **Synthesis of nanomaterials by the impulse plasma in liquid**

Chapter 1
Preface

1.1 Introduction

1.1.1 Nanomaterials

It is accepted to consider under the nanocrystal, nanostructural, nanophase materials (NM) such materials, which size of crystallites or grains or particles that form their structural base, does not exceed 100nm (1000 Å) at least in one dimension. Nanomaterials can be metals, ceramics, polymeric materials, or composite materials. The unit of nanometer derives from a Greek word "nano" meaning dwarf or extremely small. One nanometer spans 3-5 atoms lined up in a row. By comparison, the diameter of a human hair is about 5 orders of magnitude larger than a nanoscale particle. Nanomaterials are not simply another step in miniaturization, but a different arena entirely: the nanoworld lies midway between the scale of atomic and quantum phenomena, and the scale of bulk materials. At the nanomaterial level, some material properties are affected by the laws of atomic physics, rather than behaving as traditional bulk materials do.

These materials, notable for their extremely small feature size, have the potential for wide-ranging industrial, biomedical and electronic applications. As a result of recent improvement in technologies to see and manipulate these materials, the nanomaterials field has seen a huge increase in funding from private enterprises and government, and academic researchers within the field have formed many partnerships.

Wide interest to the nanomaterials have arisen in the middles of 80ties of the XX century by the works of Gleiter and the coworkers, who firstly paid attention on increasing the role of part's surfaces, especially, boundary areas by decreasing the size of a grain and offered the obtaining method of nanomaterials [1,2]. This method was consisted in the combination of making the ultradisperse powders by evaporation-condensation and their further vacuum consolidation at the high pressures. The method of Gleiter was taken for equipment in the many countries, firstly in the USA [3,4].

In 1991 S. Iijima of NEC in Japan reported the first observation of carbon nanotubes [5], which are now produced by a number of companies in commercial quantities.

Editors of the journal *Science* profiled work that resulted in molecular-sized electronic circuits as the most important scientific development in 2001 [6]. It is clear that researchers are merely on the threshold of understanding and development, and that a great deal of fundamental work remains to be done.

Top-down and bottom-up are two distinct concepts for realizing structures and devices in nanometer scale. Top-down approaches start from bulk materials, which are sculpted into nanosized features by carving, milling, etching and patterning. Lithography methods are typical examples of this approach and have been dominating technique in microelectronic engineering for fabricating integrated circuits (ICs). Controlled by powerful computers and software, a device dimension, location and organization can be achieved with a very high precise. However, inevitably, the high precision always comes at a high cost, especially when the size is below 100 nanometers. Fortunately, in the nature, there are many good examples in overcoming this challenge: in biological systems, the genetic codes and sequence guide and control the self-assembling process of supermolecules or proteins for forming higher level more complex functional and living structures. This is the bottom-up approach-constructing structures or devices from the basic building blocks, such as atoms, molecules and supermolecular clusters. This level has been the most active area in nanotechnology and a large variety of morphologies has been discovered or created. By understanding the physics and chemistry behind the growth, the ultimate goal is to control with atomic precision the morphology, structure, composition and size of nanoscale materials, so as to enable precise control over the properties of the resulting nanomaterials.

1.1.2 Nanomaterials synthesis methods

Research and development of new methods for physical-chemical processes and synthesis of chemical compounds is an important scientific technological problem. In this respect, there have been achieved great successes by using the different types of energy (plasma jets, accelerated electron beam, shock wave, laser irradiation and so on), on the basis of which new scientific fields such as plasma chemistry, electron beam technology, laser technology have appeared.

A variety of methods have been developed for synthesizing various nanostructures.

Broadly, these methods can be divided into vapor deposition techniques and solution-based chemistry techniques. Within vapor deposition, there is a physical vapor deposition and chemical vapor deposition and each method can be subdivided into more specific individual techniques. These synthesis techniques represent the majority of all techniques used for synthesizing nanomaterials.

Vapor deposition, whereby a vapor is created and is deposited on a deposition substrate, is the most common type of synthesis method. It can be divided and considered based on the method in which the depositing vapor is created. That is, vapor deposition techniques are organized based on if the vapor is created through a physical process or through a chemical process.

Physical vapor deposition (PVD) is a process in which the vapor is created in a physical manner. The three most important techniques are sputtering, pulsed laser deposition, and thermal evaporation. But they share in common that the source material is the same as the intended depositing material and no chemical reactions occur throughout the process. The main characteristics of these techniques and their disadvantages are summarized in the table 1-1.

As one of the physical methods, electrical discharge (arc, spark, glow, etc) has also been used for the synthesis of nanomaterials, especially, carbon nanomaterials such as fullerenes, carbon nanotubes, etc. In the electrical discharge methods for nanomaterials synthesis, nanoparticles are formed from the plasma produced by the electrical discharge between two electrodes in gas, however, instead of deposition to a substrate, nanoparticles are collected in the form of powders.

Arc discharge in liquid seems to be most economic and simple among the physical methods for production of various kinds of nanomaterials such as metal particles, metal nitrides/carbides/oxides [7-9], carbon onions [10] and carbon nanotubes [11-13]. However, arc discharge produces continuous plasma, which causes rapid evaporation of liquid and aggregation of formed nanoparticles into large-size particles due to the inefficient quenching of high temperature plasma. In addition, this method needs high electrical energy and induces fast increase of high temperature, which requires cooling and other safety systems.

1.2 A new method for nanomaterials synthesis

Here we introduce a new method for nanomaterials synthesis based on the low voltage spark discharge in dielectric liquids [14,15]. Low-voltage spark discharge in liquid dielectrics is one of the efficient high-energies that can intensively destroy crystal lattices of any hard conducting materials. Impulse plasma is created between two electrodes submerged into a dielectric liquid by the low voltage spark discharge. Term "impulse" in electronics is used for description of sharp transient and also pulsed phenomena. Therefore, impulse plasma is pulsed, fast and sharp plasma, which is referred to the spark discharge. In some of our papers, the word "pulsed plasma" was also used.

Impulse plasma appears from inter-electrode space break-down in high potential difference between two electrodes and relatively small output of power supply that is insufficient to excite an arc discharge. The impulse plasma in liquid method can generate pulsed plasma with duration of a single impulse less than 10 μs. The temperature in the discharge channel can reach even 10^4-10^5 K [16]. Thus, the energy of the impulse plasma can evaporate and melt any refractory (hard to melt) metal. Moreover, due to the short duration and locality of the discharge, the high temperature and pressure generated in the discharge channel are focused in a small area. Even after the several hours of the working, the temperature of the discharge liquid does not increase significantly (after 1 hour of discharge (200 V, 3 A, 0.04 J) the water temperature increases to about 1 degree). Obviously, from the formed vapor and melt, various nanoparticles of are formed. And depending on the chemical affinity, the formed nanoparticles react with the surrounding medium to form elemental particles of the electrode or compound of electrodes and the medium.

The nanomaterials of great numbers of materials can be easily synthesized by this method. In addition, nanomaterials produced by the impulse plasma in liquid have unique properties that cannot be achieved by the similar methods. The fullerene C_{60} was for the first time synthesized by electric discharge in liquid by this method. Also, we report synthesis of wurtzite ZnS by an electric discharge method for the first time. Blue amorphous TiO_2 with anatase nanocrystals was synthesized by the impulse plasma between two titanium rods in water. Copper and ytterbium nanoparticles prepared by this method were smaller than those by arc method by a factor of >5.

1.3 Features of the impulse plasma in liquid method

The impulse plasma in liquid enables us to quench from plasma state, by which we can synthesize various nanomaterials, metastable materials, etc. In addition, the applied power is 100 times smaller than those of arc discharge. The apparatus of the impulse plasma in liquid is very simple and does not require vacuum system, high-energy, cooling system, etc.

The chemical composition of the final product depends only on the electrode material and the discharge liquid so that high purity samples can be easily achieved. In addition, phase composition of the desired sample can be controlled by choosing the appropriate discharge medium or electrode materials.

Due to the short duration and locality of the discharge, the high temperature generated in the discharge channel are focused in a small area and does not cause temperature increase in the electrode or the surrounding liquid. Thus, the cooling system, which is usually required for the nanomaterials synthesis methods by electric discharge, is not needed.

So, the main advantages of the impulse plasma in liquid methods can be summarized as follows:

1. short duration of the discharge and the surrounding liquid would enable us to quench from the plasma state that lead to synthesis of metastable phases;
2. ultrafast quenching of the nascent particles result to formation of nanoparticles with very small sizes (3-5 nm);
3. no need for vacuum: reactions take place inside the chosen liquid medium (toluene, water, and so on);
4. no need for cooling system; due to the short duration and locality of the discharge, the high temperature generated in the discharge channel are focused in a small area;
5. simplicity of the methods and the apparatus, which can be easily scaled up;
6. low cost of the product.

1.4 Purpose of the present study

Nanoscience and nanotechnology is a relatively new field of research. Nanomaterials

science is an interdisciplinary subject. Thus, it requires involvement of many research fields such as physics, chemistry, materials science, etc. Even though a huge number of researches have been conducted in the area of the nanomaterials research, the fundamental questions of the nanomaterials formation mechanism poorly understood. In addition, despite the large number of synthesis techniques for the nanomaterials synthesis, high quality samples with higher performance and low cost is still challenging. Synthesis and characterization of the nanomaterials by a new synthesis method would increase the knowledge of formation mechanism of the nanoparticles for the more precise control over the phase composition, morphology, crystal defects, etc of the desired nanomaterials. In addition, application of the spark discharge submerged in liquid for the synthesis of nanomaterials was not studied before.

Therefore, the purpose of this study was to develop a new method for the nanomaterials synthesis using the impulse plasma in liquid and their characteristics by the state-of-the-art research equipment available. We have studied the formation of carbon nanostructures, metallic and oxide nanoparticles by the impulse plasma in liquid method by using the different combinations of electrodes, different discharge solutions and various experimental parameters such as frequency, impulse energy, etc.

1.5 Summary of this work

A new synthesis method for nanomaterials using the impulse plasma in liquid by the low voltage spark discharge is presented. Design and production of a new apparatus for the impulse plasma in liquid is described. Power for the device is supplied by inverter with adjustable frequency between 1-1500 Hz, voltage of 50-200 V, and current up to 20 A. This method has many advantages that provide powerful capability and efficiency for the nanomaterials synthesis. The fullerene C_{60} and wurtzite ZnS nanoparticles were for the first time synthesized by the electric discharge method in liquid, i.e. by our method. The purity of C_{60} was > 99 %, which is much higher than those by the conventional arc plasma in inert gas methods (less than 80 % C_{60} and 20 % C_{70} and other fullerenes). Wurtzite ZnS nanoparticles with a diameter of about 5 nm were produced by a novel catalyst-free, low temperature method. It was found that the wurtzite ZnS nanoparticles have stacking faults even without any additional treatment. Therefore, it is expected that this material exhibits

better photoluminescence property. Shock wave compression of ZnMgS powder also created crystallographic defects and induced the phase transition of ZnS from zinc blend to wurtzite type structure. Photoluminescence spectrum of ZnMgS sample was improved by the shock compression. Blue amorphous TiO_2 with anatase nanocrystals was synthesized by the impulse plasma between two titanium rods in water. UV-vis absorption spectra of the blue anatase TiO_2 nanopowder showed higher absorbance in the visible spectral region than the commercial anatase photocatalyst. Metallic nanoparticles of copper and ytterbium were prepared by the impulse plasma in styrene. Copper nanoparticles prepared by this method were smaller than those by arc method by a factor of >5. The impulse plasma in liquid enables us to quench from plasma state, by which we can synthesize nanomaterials, metastable materials, etc.

In the *Chapter 1*, the importance of this study, comparison of the existing nanomaterials synthesis methods, introduction of the new method, the features of the impulse plasma in liquid, the purpose of this work were described.

In the *Chapter 2*, the description of the new synthesis method for nanomaterials by the impulse plasma in liquid was given. The production and installation of the new apparatus of the impulse plasma in liquid method was described. Waveforms of the discharge current and voltage were measured using the digital oscilloscope. The electrical components and design of the circuit was reported. Some safety measurements to be taken during the experiments with the impulse plasma in liquid apparatus were briefly given.

In the *Chapter 3*, the preparation of metallic nanoparticles of copper and ytterbium by the impulse plasma in liquid method was described. Metallic particles of copper and ytterbium were synthesized by the impulse plasma between copper and ytterbium electrodes respectively, submerged into styrene. Transmission Electron Microscopy (TEM) analysis showed that copper nanoparticles prepared by the impulse plasma in styrene were smaller than those by arc discharge in CTAB/ascorbic acid solution by a factor of >5. Such a small size of the formed nanoparticles was related to the formation of the polymer protective shell, which is coated on the surfaces of the nascent nanoparticles.

In the *Chapter 4*, the synthesis of the fullerene C_{60} by the impulse plasma in liquid was reported. This is the first report on the synthesis of fullerene C_{60} by the electric discharge in liquid. Impulse plasma between two graphite electrodes submerged in toluene produced fullerene solution and black soot at the bottom. The analysis of the solution by the High Performance Liquid Chromatography revealed that the sample contains of

fullerene C_{60}. The purity of C_{60} was > 99 %, which is much higher than those by the conventional arc plasma in inert gas methods (less than 80 % C_{60} and 20 % C_{70} and other fullerenes). The black soot reflected the similar X-Ray Diffraction (XRD) peaks with the fullerene soot produced by the arc discharge in argon. Even though the phase composition of the sample produced at the different frequency remained the same, increasing the frequency of the impulse plasma resulted in the increasing the formation of the small sized particles.

In the *Chapter 5*, the synthesis of blue colored amorphous TiO_2 nanoparticles was reported. The impulse plasma between titanium rods in water produced blue solution and black particles at the bottom. XRD analysis revealed that the blue particles separated from the blue solution are amorphous and the black particles consist of TiO phase. High Resolution Transmission Electron Microscopy (HRTEM) analysis showed that the blue amorphous TiO_2 contains the anatase nanocrystals with less than 10 nm size. Annealing of the blue amorphous nanoparticles resulted in formation of anatase structure TiO_2 at low temperatures (300-400 ℃) and rutile phase at the higher annealing temperatures (500-800 ℃). The blue color of the sample gradually changed to white starting from 500 ℃ and turned to white at 800 ℃. By increasing the temperature of water, the phase composition of the blue particles remains the same except small increase of the crystallinity. The absorption spectra of the blue amorphous TiO_2 showed high absorption in the visible light range. It is expected that this sample exhibits excellent photocatalytic properties under the visible light. The experiments on the photocatalytic property of the blue amorphous TiO_2 under the UV light showed that the annealed at 400 ℃ blue amorphous TiO_2 sample has higher photocatalytic property than the commercial anatase photocatalyst.

In the *Chapter 6*, the synthesis of wurtzite structure ZnS by a catalyst-free, low-temperature method was described. This is the first report of the synthesis of ZnS by an electric discharge method. Impulse plasma between two zinc electrodes in sulfur formed the wurtzite ZnS and metallic Zn particles. HRTEM analysis revealed that the sample contains hexagonal ZnS nanocrystals of about 10 nm. Impulse plasma between two zinc electrodes in sulfur caused the formation in ZnS nanocrystals the crystallographic defects (stacking faults), which are usually concerned as an intensifier of the photoluminescence property. Changing one of the electrodes to magnesium caused the formation of MgS additionally to ZnS and Zn nanoparticles.

TEM analysis of the sample treated by the shock wave at the impact velocity of 0.68

km/s did not show any significant change of the crystal state. However, powders treated by the shock wave with the impact velocity at 1.0 km/s and 0.91 km/s were successfully compacted and were hard enough. The crystallographic defects (stacking faults) were created in some ZnMgS particles by the shock loading. This resulted in the improvement of the photoluminescence and shifting the emission wavelength to the UV spectral range.

In the *Chapter 7*, general conclusions of the present study were summarized.

References:

[1] H. Gleiter. Proc. II Riso Int. Symp. Metallurgy and Mater. Sci., 1981, 15

[2] R. Birringer, U. Herr, H. Gleiter. Suppl. Trans. Jpn. Inst. Metals 27, 1986, 43

[3] R. Siegel, H. Hahn. Curr. Trends in the Phys. Mater., 1987, 403

[4] G. Saito, T. Teramoto, A. Otsuka, Y. Sugita, T. Ban, M. Kusunoki, K. Saraguchi. Synth. Met. 64, 1990, 359

[5] S. Iijima, Nature 354, 1991, 56

[6] Science, 294, 5551, Science, 294, 2442-2443

[7] T. Satsuta, M. Hasegawa, N. Harada, S.J. Asai, J. Japan Inst. Metals 1993, *57,* 296.

[8] T. Sato, K. Usuki, A. Okuwaki, Y. Goto, J. Mater. Sci. 1992, 27, 3879.

[9] S.Y. Xie, Z.J. Ma, C.F. Wang, S.C. Lin, Z.Y. Jiang, R.B. Huang, L.S. Zheng, J. Solid State Chem. 2004, 177, 3743.

[10] N. Sano, H. Wang, I. Alexandrou, M. Chhowalla, K.B.K. Teo, G.A.J. Amaratunga, K. Iimura, J. Appl. Phys. 2002, 92, 2783.

[11] Y.L. Hsin, K.C. Hwang, F.-R. Chen, J.-J. Kai, Adv. Mater. 2001, 13, 830.

[12] H.W. Zhu, X.S. Li, B. Jiang, C.L. Xu, Y.F. Zhu, D.H. Wu, X.H. Chen, Chem. Phys. Lett. 2002, 366, 664.

[13] H. Lange, M. Sioda, A. Huczko, Y.Q. Zhu, H.W. Kroto, D.R.M. Walton, Carbon 2003, 41, 1617.

[14] E. Omurzak, J. Jasnakunov, N. Mairykova, A. Abdykerimova, A. Maatkasymova, S. Sulaimankulova, M. Matsuda, M. Nishida, H. Ihara, T. Mashimo, J. Nanosci. Nanotechnol. 2007, 7, 3157

[15] E. Omurzak, M. Matsuda, H. Ihara, T. Mashimo, S. Sulaimankulova. Adv. Mater. Res. 15-17 (2007), 549

[16] S. Sulaimankulova, U. Asanov. Energy-saturated media in the spark discharge plasma. Bishkek. 2002

Table 1-1. Advantages and disadvantages of nanomaterials synthesis techniques

Method	Advantages	Disadvantages
Sputtering	An advantage of sputtering as a deposition technique is that the deposited films have the same composition as the source material. The equality of the film and target stoichiometry might be surprising since the sputter yield depends on the atomic weight of the atoms in the target. One might therefore expect one component of an alloy or mixture to sputter faster than the other components, leading to an enrichment of that component in the deposit.	However, since only surface atoms can be sputtered, the faster ejection of one element leaves the surface enriched with the others, effectively counteracting the difference in sputter rates. In contrast with thermal evaporation techniques one component of the source may have a higher vapor pressure, resulting in a deposited film with a different composition than the source.
Pulsed Laser Deposition	Easy to implement: a laser beam vaporizes a target surface, producing a film with the same composition as the target. It is versatile: many materials can be deposited in a wide variety of gases over a broad range of gas pressures. Greater control of growth (e.g., by varying laser parameters)	• uneven coverage • high defect or particulate concentration • not well suited for large-scale film growth • high cost
Chemical Vapor Deposition (CVD)	• high growth rates possible • can deposit materials which are hard to evaporate • good reproducibility • can grow epitaxial films	• high temperatures • complex processes • toxic and corrosive gasses
Thermal CVD	Thermal CVD is typically used to form thin films. Thermal CVD can occur between two gas phase precursors or between a gas phase precursor and a solid phase precursor.	Thermal CVD requires pressure near 10^{-3} Torr. It is limited by its high required temperatures and the slow deposition rates

Table 1-1. continued

Molecular Beam Epitaxy (MBE)	Precise control of the thickness of each layer, down to a single layer of atoms. The most important aspect of MBE is the slow deposition rate, which allows the films to grow epitaxially	The slow deposition rates require proportionally better vacuum in order to achieve the same impurity levels as other deposition techniques. The process takes place in high vacuum or ultra high vacuum.
Atomic Layer Deposition (ALD)	• in theory ALD allows for atomic level control of thin film thickness and uniformity ▪ stoichiometric films with large area uniformity ▪ precise thickness control ▪ low temperature deposition possible ▪ gentle deposition process for sensitive substrates	The precursor adsorbs until it saturates the surface and further growth cannot occur until the second precursor is introduced. Thus the film thickness is controlled by the number of precursor cycles rather than the deposition time as is the case for conventional CVD processes.
Solution based chemistry	Any chemical reaction that requires a solution to occur is a form of solution based chemistry (SBC). Often, some materials with complex stoichiometries are difficult to synthesize via vapor deposition techniques. In these situations, SBC has served as a vital technique in producing these materials.	SBC techniques typically provide materials with high yield and uniformity, but a major disadvantage is that there are more point, line, and planar defects than there are in vapor deposition created materials.
Sol-gel	• ultra-fine powders, monolithic ceramics and glasses, ceramic fibers, inorganic membranes, thin film coatings and aerogels • lower processing temperatures • lower costs	▪ long processing times ▪ preferential hydrolysis ▪ precursors ▪ additives

Chapter 2
Impulse plasma in liquid

2.1 Introduction

Plasma in liquid, i.e. impulse plasma in liquid is created by the low voltage spark discharge that arises from the inter-electrode gap breakdown in the high potential difference between two electrodes submerged into a dielectric solution. One of the features of the spark discharge is that the current density in the spark channel and the electrode surface is high and can reach order of 10^5-10^7 A/mm^2 [1]. The developed temperature by spark channel during discharge can evaporate any refractory metal or alloy. But such destructions are localized in a small area and the duration of high-temperature impulses are short. Owing to this, the surrounding medium remains in liquid state having affected only in the discharge channel [2,3].

The above-mentioned and those listed in the previous chapter features of the impulse plasma are more than enough for application of this kind of discharge in carrying out chemical processes such as synthesis. Ejected by the spark discharge metal particles (vapor, melt, ions, etc) actively react with the components of the dielectric liquid. Depending on the chemical composition of initial liquid dielectric and chemical affinity of its components with the electrode materials, either individual metallic or mixture of different metal compounds can be formed.

Chemical synthesis in these conditions has effective quenching and as a consequence high temperature and metastable phases can be formed. Synthesis of nanomaterials that cannot be easily produced by the existing synthesis methods or even new materials also is expected.

We have developed a new synthesis method for nanomaterials and produced some nanomaterials using this method [4-6].

2.2 Method

Figure 2-1a represents the schematics of our apparatus with a photograph of the impulse plasma created between two electrodes submerged into liquid. Main parts that play an important role in the creation of impulse plasma are: (a) electrical parameters of the circuit (voltage V, current I, capacitance C) and (b) conductance of electrode materials and the dielectric liquid. By increasing the value of the electrical parameters, the energy of the impulse plasma increases: consequently the plasma temperature increases, UV light becomes brighter, shock wave stronger. By changing the dielectric liquid, we can obtain either element or oxide particles. Vacuum system and cooling system, which are used in the nanomaterials and fullerene production methods [7-9] by arc discharge, are replaced by dielectric (toluene, water, so on) solutions. One of the electrodes was kept vibrating in order to keep the discharge process stable. Without vibration of the electrode, the discharge process continues just for a while and ceases until the gap between the electrodes is adjusted again. The bottom graphs of the Figure 2-1 show the waveforms of discharge current in different time scales. Duration of a single discharge is estimated to be less than 10 μs (Figure 2-1c). By changing the discharge parameters (voltage, impulse energy), the production rate can be changed.

Integral quantity of the destroyed material (Γ) during the impulse plasma can be described by the sum of the spark effects of the every single pulse

$$\Gamma = \sum_{i=t}^{N} \gamma_i \quad (2.1)$$

where N – is number of the impulses

γ – is the value of destructibility

quantity of the destroyed material is proportional to single pulse energy

$$\gamma = KE, \; E = \frac{CU^2}{2} \quad (2.2)$$

where K – is a coefficient of proportionality

E- is energy stored in the condenser, J

C- condenser capacity, F

U – charging voltage, V

Energy of a single impulse is controlled by changing the capacity of the condensers, value of the charging voltage. We have chosen a single impulse energy and dielectric liquid for the discharge depending on the being dispersed material's properties: boiling point of the electrode materials and chemical affinity of liquid with the electrode. For the materials that have high melting point, higher capacitance and voltage is required. The solubility of fullerenes is high in toluene, so we have used toluene as a reaction liquid. Similarly, for copper and ytterbium, styrene was chosen to prevent the forming powder from oxidation. Water was used to obtain titanium dioxide and sulfur for ZnS.

Due to small energy-intensiveness that is conditioned by locality of the single plasma impulse, its small duration and placement of electrodes into a liquid, the system has no need for cooling system. This is conditioned by small duration of a single impulse that does not cause high temperature widening or significantly moving on the electrode surface.

Main advantages of the impulse plasma are:

1. Metastable states can be formed due to short discharge time
2. Ultrafast quenching enables preparation of nanoparticles less than 10 nm
3. Applied power is 100 times smaller than that of arc discharge
4. Simple equipment design, which can be easily scaled-up
5. No need for vacuum (reactions take place inside a certain liquid)
6. Temperature increase in discharge zone is low: cooling is not necessary

2.3 Apparatus

2.3.1 Parts of the electrical circuit

Figure 2-2 shows a photograph of the impulse plasma in liquid apparatus. The impulse plasma generator consists of electrical circuit, power source and discharge chamber. In the design of the circuit, priority was given to the safety side.

All parts of the circuit were purchased separately and assembled in a 600x500x250 mm sized metal case manually by ourselves.

Inverter Hitachi SJH300-16LF was used as the power source for the impulse plasma. From the Figure 2-2, we can see the inverter in between the discharge chamber and the electric circuit. The output parameters of the inverter are as follows: 0.1-1500 Hz, AC 200-240 V, 3 phase, 46 A. The current was limited by resistors up to 20 A.

The working principle of the circuit is simple: the condenser is charged by 200 V from the inverter. When the thyristor opens, the charged energy in the condenser is discharged to the gap between the electrodes submerged into a liquid, so we can get the pulsed plasma.

For the safety from the gases coming out from the liquid surface during the discharge process, the beaker was placed inside a fume hood. Toxic or flammable gases produced during the impulse plasma are blown out by the fume hood fans. After the electrodes fixed and submerged into the discharge liquid, the fume hood is closed and the power is applied.

The electrodes are fixed in the shape of V and submerged into liquid. One of the electrodes was held by the electrically isolated clamps and fixed to the stand. Another electrode was fixed to vibrator and was vibrated within 3 mm amplitude. Electrode tips were held inside the liquid with more than 30 mm depth from the top of liquid surface. Usually 200 ml or 500 ml beakers made of glass were used for carrying out the discharge.

2.3.2 Voltage and current of the impulse plasma

The waveforms of the current and voltage were measured by the digital oscilloscope by the scheme shown in Figure 2-1. CT stands for current transformer, i.e. Rogowsky coil for the measurements of the current waveforms. VP – is the voltage probe made by ourselves, which consists of two resistors of 50 Ω and 20 kΩ and was used for the voltage measurements. Typically the AC power supply has the sine wave as in the upper graph in the Figure 2-3. The output waveforms of the impulse plasma voltage and the current between the electrodes are shown in the lower graph in the Figure 2-3. Figure 2-4 shows the discharge current and voltage in different time scales. We can see that the discharge current is pulsed. From the Figure 2-4c, the duration of the single impulse plasma was measured to be about 10 μs. The discharge waveform shows usual behaviour typical to the low voltage spark discharge, when the current increases the voltage decreases as shown in the Figure 2-4c and 2-4d.

2.4 Health and safety measurements

As the impulse plasma involves high electric power which can seriously damage and can lead to fatal electric shock. It can cause cardiac arrest or muscular spasms, and

pathway - if the current passes through the chest or head there is an increased chance of death. It is sometimes suggested that human lethality is most common with alternating current at 100-250 volts, however death has occurred from supplies as low as 32 volts and supplies at over 250 volts frequently cause fatalities.

On the other hand, recently the concerns about the nanoparticles hazard to human health are increasingly growing. Although, it is not proven that every nanosized material is hazardous, researchers discovered that exposure to TiO_2 dramatically broke down the cellular layer, indicating that the nanomaterial either killed the cells or weakened the cellular junctions. What is needed at this time is a concerted effort to make safer the working place and environment by all available means.

Refer to the health and safety manual published recently (2006) by the Kumamoto University or other information sources for more instructions for safety.

2.5 Conclusions

Impulse plasma in liquid by the low voltage spark discharge is a new synthesis method for the nanomaterials. So far reported physical nanomaterials synthesis methods are mainly based on arc discharge. Arc discharge causes transformation of formed nanoparticles into large clusters. Impulse plasma has an advantage such as short duration of discharge process that allows fast quenching of metastable states formed during discharge and fixes non-equilibrium phases. By changing the dielectric liquid, we can obtain either metallic particles, carbides or oxides of a metal.

A new apparatus of the impulse plasma in liquid method apparatus was successfully produced and installed at the Kumamoto University. In the design of the circuit, priority was given to the electrical and health safety. All parts of the circuit were purchased separately and assembled in a 600x500x250 mm sized metal case. Power for the device is supplied by inverter with adjustable frequency between 1-1500 Hz, voltage of 50-200 V, and current up to 20 A.

The discharge current and voltage waveforms were measured by the digital oscilloscope. The duration of a single impulse was measured to be 10 μs. Impulse Plasma device can generate impulse plasma of 10 μs duration with up to 100 mJ impulse.

References

[1] N.K. Foteev. Spark processes metal. Moscow, Znanie, 1967

[2] U. Asanov. Physical-chemical processes in spark discharge plasma in liquid dielectrics. Frunze, Ilim, 1978

[3] S. Sulaimankulova, U. Asanov. Energy-saturated media in the spark discharge plasma. Bishkek, Kyrgyzpatent, 2002

[4] E. Omurzak, J. Jasnakunov, N. Mairykova, A. Abdykerimova, A. Maatkasymova, S. Sulaimankulova, M. Matsuda, M. Nishida, H. Ihara, T. Mashimo, J. Nanosci. Nanotechnol. 7, 2007, 3157

[5] E. Omurzak, S. Sulaimankulova, T. Mashimo. Review of High Pressure Science and Technology 16, 2006, pp.281

[6] U.A. Asanov, J.K. Jasnakunov, E. Omurzak, S.K. Sulaimankulova. Selected works of the National Academy of Sciences of the Kyrgyz Republic (journal's 50th anniversary issue), 2004, pp.21-31

[7] H.W. Kroto, J.R. Heth, S.C. O'Brien, R.F. Curl, R.E. Smalley, Nature 318, 162 (1985)

[8] W. Kratschmer, L.D. Lamb, K. Fostiropoulos, D.R. Huffman, Nature 347, 354 (1990)

[9] F. Gao, S.Y. Xie, R.B. Huang, L.S. Zheng. Chem. Commun. 2676 (2003)

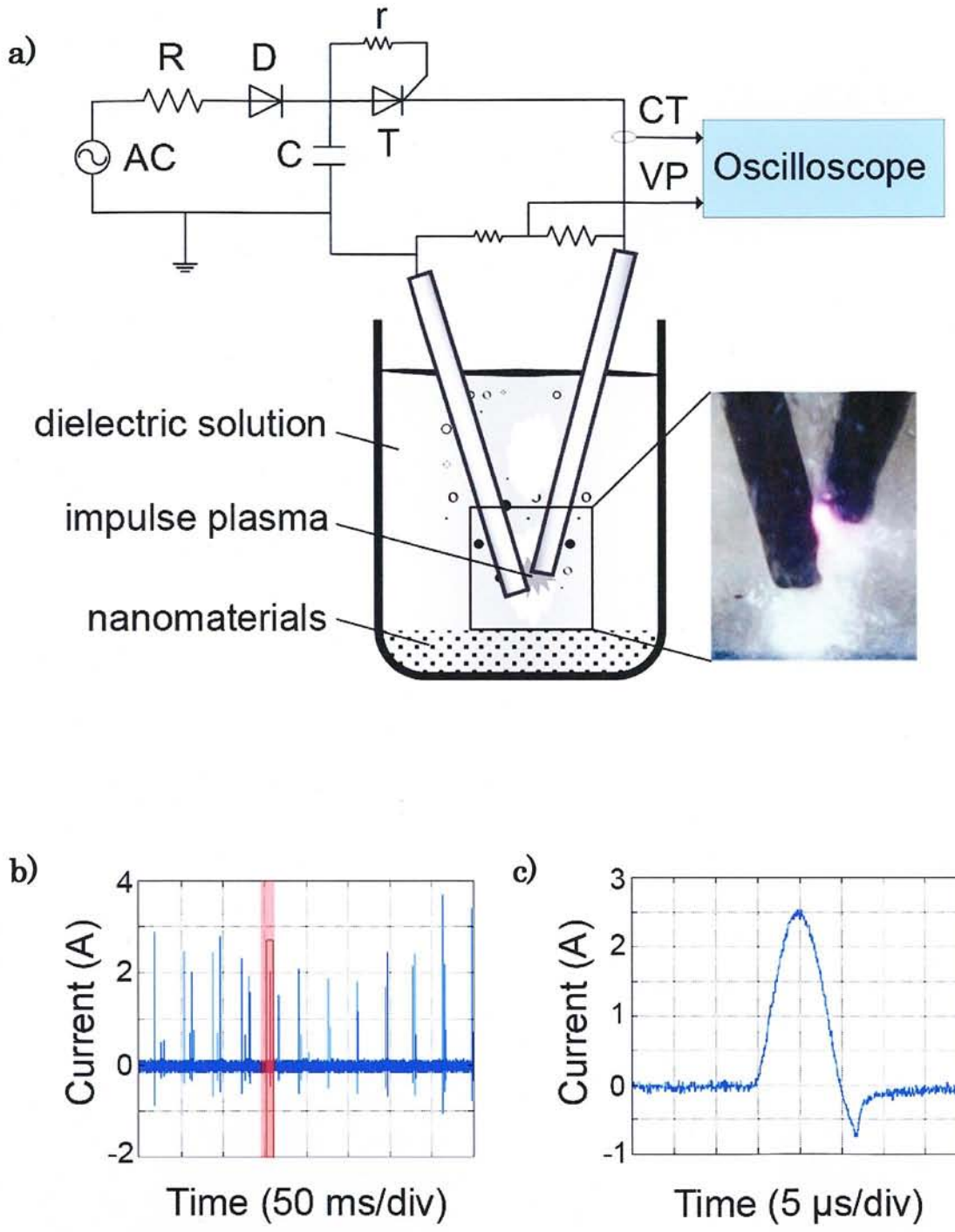

Figure 2-1. a) Schematics of the impulse plasma in liquid with a photograph of discharge, b) waveforms of discharge current and (c) enlarged view

Figure 2-2. Photograph of the impulse plasma in liquid apparatus

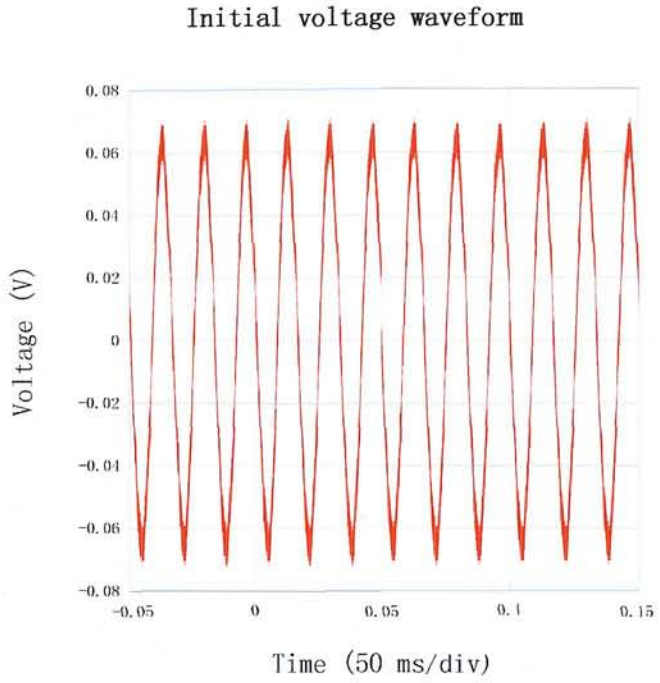

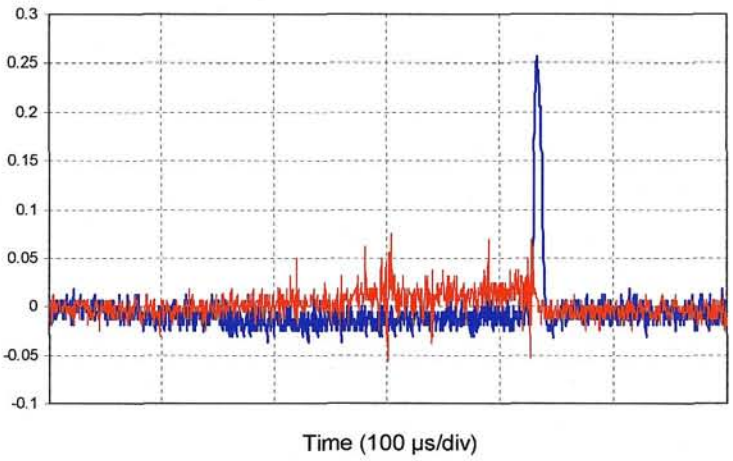

Figure 2-3. Typical sinusoidal waveform of the input AC voltage. The bottom figure represents the output waveforms of the current (blue line) and voltage (red line)

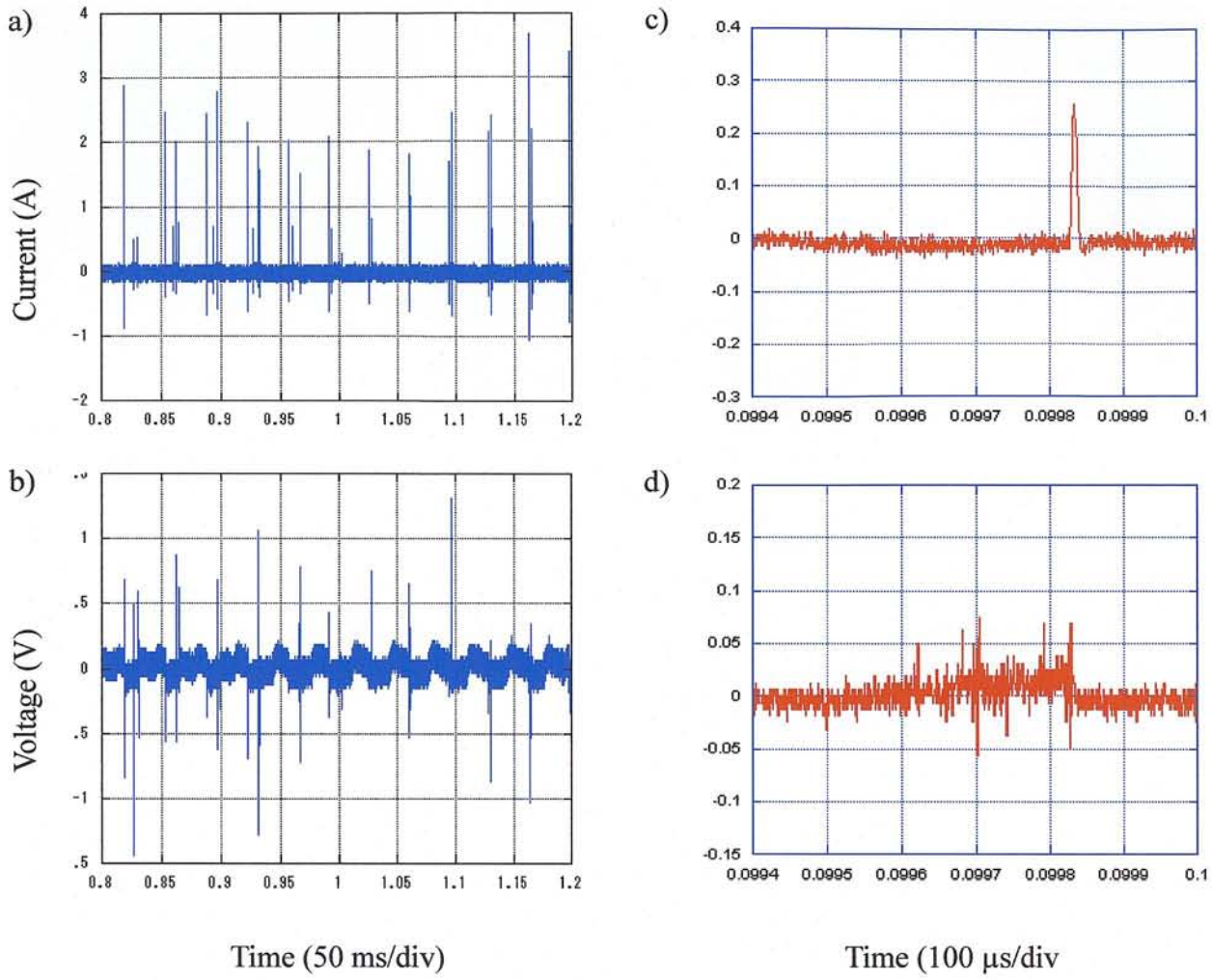

Figure 2-4. Waveforms of the impulse plasma generator with the time resolution of 50 ms/div current (a) and voltage (b) and the single impulse waveforms of current (c) and voltage (d)

Chapter 3
Metal nanoparticles

3.1 Synthesis of metal nanoparticles

Metal nanoparticles preparation methods can be mainly classified into two kinds of processes, i.e., physical and chemical [1-3]. The physical approach is versatile towards a wide range of metal nanoparticles with high quality, but it usually calls for expensive vacuum systems and high electric power to generate plasmas. The chemical route appears to be capable of controlling growth and assembly of metal nanoparticles by optimizing reaction parameters (e.g., surfactant, capping agent, solvent, precursor concentration and temperature), but is mainly employed to synthesize nanomaterials of noble metals such as Ag and Au [4-6]. In addition, chemical synthesis methods for metal nanoparticles consume toxic chemicals, which are not desirable for the ecological reasons. Therefore, combination of physical and chemical processes should be realized to develop a new flexible method for the preparation and assembly of different metal nanoparticles. Recently, the arc-discharge in liquid phase (cetyltrimethylammonium bromide (CTAB)/ascorbic acid solution) for the synthesis of copper particles was reported [7]. However, arc discharges caused the aggregation of the forming nanoparticles into the large particles (about 1 micron).

Here we presented a new synthesis method for metal nanoparticles by the impulse plasma in liquid [8-10].

3.2 Experimental procedure

For copper, two electrodes made from 6 mm pure copper rods submerged into 200 ml pure styrene. One of the electrodes was kept vibrating during the discharge process in order to keep the impulse plasma stable. The discharge voltage and current were 200 V and 1 A respectively. After the impulse plasma applied to the electrodes for about 3 hours, copper particles formed about 3 gram powder at the bottom. Formed powder was filtrated and

dried in an inert atmosphere. Ytterbium dispersion has also the same procedures and has about the same production rate of 1 g/h.

Figure 3-1 represents the experimental process scheme after the impulse plasma was applied. After the impulse plasma is stopped, the solution was left for natural sedimentation of the heavier particles for about an hour unless it requires more time for sedimentation. After that the solution was decanted. The solution was further taken for separation of the particles from the liquid by centrifuge, filtration or extraction by the Soxhlet apparatus. Then both the sediment and centrifuged or extracted samples were analyzed.

XRD patterns of the samples were taken using Cu-Kα radiation, Rigaku RINT-2500VHF. The electron microscopy images of the products were taken by Transmission Electron Microscope (TEM) JEOL-200FX: some amount of powder samples were dropped to methanol solution and were ultrasonicated for 3 minutes. Then the particles were collected by copper grids (200 mesh) and were dried in air for TEM observations.

3.3 Results and discussion

3.3.1 Cu and Yb nanoparticles

Figure 3-1 shows the XRD pattern of the sample produced by the impulse plasma between two ytterbium electrodes in styrene (a) and XRD pattern of the initial bulk ytterbium (b). We can see that XRD analysis of this sample (Fig. 3-1a), revealed the reflexes of (111) and (200) planes, which correspond to the metallic ytterbium with fcc lattice like copper's. For comparison, the XRD pattern of bulk ytterbium is given in Figure 3-1b. Analysis shows that the formed powder consists of metallic nanoparticles of ytterbium with the average particle sizes of 25-30 nm.

Figure 3-2 shows the XRD patterns of the sample produced by the impulse plasma between two copper electrodes in styrene (a) and initial bulk copper (b). XRD analysis showed that dispersion of bulk copper by impulse plasma in styrene resulted in formation of metallic nanoparticles of copper. As prepared nanostructures are particles of copper with fcc structure (spatial group O_h^5-Fm3m, Z-4). Crystal lattice of copper after the discharge (a=3.6215Å) slightly widened comparing to a bulk one (a_{mass}=3.6147 Å). Particle size of the copper nanoparticles was estimated by the Scherrer's formula to be 3-4 nm. At the

bottom in the Fig. 3-2, TEM image of the copper particles formed by the impulse plasma between two copper electrodes in styrene is shown. Very small particles of about 3 nm were observed.

Accordingly, the dispersed from the tips of electrodes copper/ytterbium ions immediately react with the surrounding styrene that lead to forming of metallic nanoparticles and prevent from oxidation.

3.3.2 Nanoparticles formation mechanism

Mechanisms for the nanoparticles formation in the impulse plasma in liquid have not been well understood yet. Since the impulse plasma and arc discharge have similar nature, we explain the formation mechanism in the impulse plasma by comparing it with the reported models for the arc discharge in water. Figure 3-3A shows the proposed formation mechanism of the carbon nanomaterials by the arc discharge in deionized water by Sano etal [11]. As mentioned earlier, arc discharge produces continuous plasma, so they divided the formation process into different zones according to the temperature gradient.

Figure 3-3B represents the nanoparticles formation mechanism by the impulse plasma in liquid method on the basis of the water arc model by Sano etal. The temperature of the hot plasma is considered to be the same with the arc plasma, however, due to fast quenching and short duration of pulses, the impulse plasma in liquid cannot develop such zones as in water arc, instead we consider different time intervals for the formation of nanoparticles. Temperature increase in the impulse plasma in liquid has very sharp peak and does not expand to the surrounding medium. So the temperature of the liquid remain equal to the room temperature, while in the water arc it increases up to the boiling point of water and even more.

During the time I, hot plasma consisting of the ions of metals is formed. Then, in the time II, gas bubbles, which can be regarded as micro reactor chamber, are formed due to vaporization of surrounding liquid and the atoms inside this micro-reactor by joining each other serve as "seeds" of particles. During the time III, the "seeds" that have sufficient activation energy grow to form nanoparticles.

We assume that during the nanomaterials formation by the impulse plasma in liquid, metallic nanoparticles are formed first. Because, the pressure developed in the spark area (3-10kBar) [12] does not allow the surrounding components to enter the micro-reactor. After the spark process ceases, the pressure inside the micro reactor falls down, and

already formed nanoparticles react with the components of the surrounding dielectric liquid due to their high activity.

3.3.3 Stabilization of the nanoparticles and forming of polymer shell

The reasons for increasing of the reactivity of the solids during their dispersion is the decreasing of the particle sizes by increasing the surface area, which lead to the increasing of the free surface energy and formation of the thermodynamically non-stable state. Freshly-formed surface of the substances are easily oxidized in air right up till the spontaneous combustion, if the formation of the particles take place without formation of the protective shell. The stabilization problem rises in the synthesis of nanoparticles, which are naturally concerned as the substances of active (energy-saturated) state.

Let us consider the formation mechanism of the polymer shell on the surface of the particles, produced by the impulse plasma in styrene. During the direct formation of the particles in a monomer, the physical-chemical characteristics of the solids have a big significance. Polymer formation activity of metals (in some particular media) directly depends on the electron emission value: larger the electron emission, larger the yield of polymer. [13]

It was found that the colloidal copper, silver and platinum slow down the styrene polymerization in any concentrations of metals [13]. Colloidal metals form as if a sprayed wall in the solution and the atoms serve as the cutters of the growing chain (similar to the radicals that have free valency). Nevertheless, the particles will be covered by a protective shell with a thickness necessary for the protection and stabilization of the colloidal or the nanoparticle.

Kinetics of the polymer shell growth was studied in relation with various factors [14]. It was shown that the shell growth speed is proportional to the intensity of the radiation and does not depend on the substrate material. The growth speed slows down by time and the formation of the shell depends on three factors:

1. vapors that can form polymer (in our case styrene);
2. surface, where the shell is being created (particle surfaces);
3. electron beam (surface of the clusters are full of electrons, defects, dislocations).

Polymer shell growth speed does not depend on the radiation time, but strongly depends on the substrate temperature. Since the surface temperature of the particle formed by the impulse plasma in liquid changes from up to down, the ionic mechanism of polymerization

of the being used monomer can be considered. Radical polymerization of the excited metal atoms can flow as follows:

$$CH_2 = CH_2 + M^* \longrightarrow CH = CH_2 + MH \quad (4.1)$$

or

$$CH_2 = CH_2 + M^* \longrightarrow CH = CH_2 + M + H \quad (4.2)$$

Most probably the styrene polymerization according to the radical mechanism will look similar, because, there is a large number of excited metallic atoms on the particle surface, especially, the surface atoms are connected each other weaker than the inner atoms.

The formation of the polymer protective shell in the conditions of the impulse plasma in liquid is natural, since the energy of the impulse plasma is enough high to destroy any metal with forming energy-saturated media. Also this energy is sufficient for the maintaining the nanoparticles in the excited state during a certain period of time, which is required for the polymerization process of any monomer. In addition, non-equilibrium state of the impulse plasma process promotes the formation of polymerization centers on the fresh particle surfaces.

Protective polymer shell was formed on the surfaces of copper nanoparticles produced by the impulse plasma between two copper electrodes in styrene (single energy 0.05 J). The copper sample was solved repeatedly in order to solve the polymer shell from the particle surfaces. The filtrated sample was studied by IR spectroscopy (400-4000 cm^{-1}). Figure 3-4 shows the IR spectra of the sample by the impulse plasma between copper electrodes submerged into styrene and the separated from the copper particles polymer shell. The IR spectrum of the polymer shell, which was solved out from the copper nanoparticles showed similar pattern with the polystyrene. This suggests that the polymer shell on the surface of the copper particles was formed.

3.4 Conclusions

In summary, we presented a new synthesis method for the copper and ytterbium nanoparticles by using the impulse plasma in liquid. The impulse plasma in liquid enables us to quench from plasma state, by which we can synthesize nanomaterials, metastable

materials, etc. Copper nanoparticles prepared by this method were smaller than those by arc method by a factor of >5. The present method can be used for the synthesis of various kinds of metal and compound nanomaterials. The protective polymer shell was formed on the surface of the particles by the impulse plasma in liquid.

References

[1] G. Schmid, Clusters and Colloids from Theory to Application, VCH, Weinheim, 1992

[2] D.L. Feldheim, C.A. Foss Jr., Metal Nanoparticles: Synthesis, Characterization, Applications, Marcel Dekker, New York, 2002.

[3] R.W. Siegel, E. Hu, M.C. Roco, Proceeding of R & D Status and Trends in Nanoparticles, Nanostructured Materials and Nanodevices, Kluwer, 1999, 19

[4] Y.G. Sun, Y.N. Xia, Science 298 (2002) 2176

[5] R. Jin, Y. Cao, C.A. Mirkin, K.L. Kelly, G.C. Schatz, J.G. Zheng, Science 294 (2001) 1901

[6] C.J. Murphy, N.R. Jana, Adv. Mater. 14 (2002) 80

[7] S.Y. Xie, Z.J. Ma, C.F. Wang, S.C. Lin, Z.Y. Jiang, R.B. Huang and L.S. Zheng, J. Solid State Chem. 177, 3743 (2004)

[8] E. Omurzak, S. Sulaimankulova, T. Mashimo. Proceedings of Annual Meeting of the Ceramic Society of Japan 2007, Tokyo, pp. 197

[9] J. Jasnakunov, E. Omurzak, S. Sulaimankulova, U. Asanov. Izvestia VUZov, Bishkek, V.8, 2004, pp.11-14

[10] E. Omurzak, J. Jasnakunov, S. Sulaimankulova, T. Mashimo. Proceedings of Symposium on the Shock Waves in Japan, Kyushu University, pp. 265-266

[11] N. Sano, H. Wang, I. Alexandrou, M. Chhowalla, K.B.K. Teo, G.A.J. Amaratunga and K. Iimura, J. Appl. Phys. 92, 2783 (2002)

[12] S. Sulaimankulova, U. Asanov. Energy-saturated media in the spark discharge plasma. Bishkek. 2002

[13] A.D. Pomogailo, A.S. Rozenberg, I.E. Ufland. Metal nanoparticles in polymers. Moscow, Chimia, 2000

[14] E.T. Murzabekova, S.K. Sulaimankulova, J. Maatkerimova. Journal of the Chemical Institute of Kyrgyzstan, 1998, 2, 191

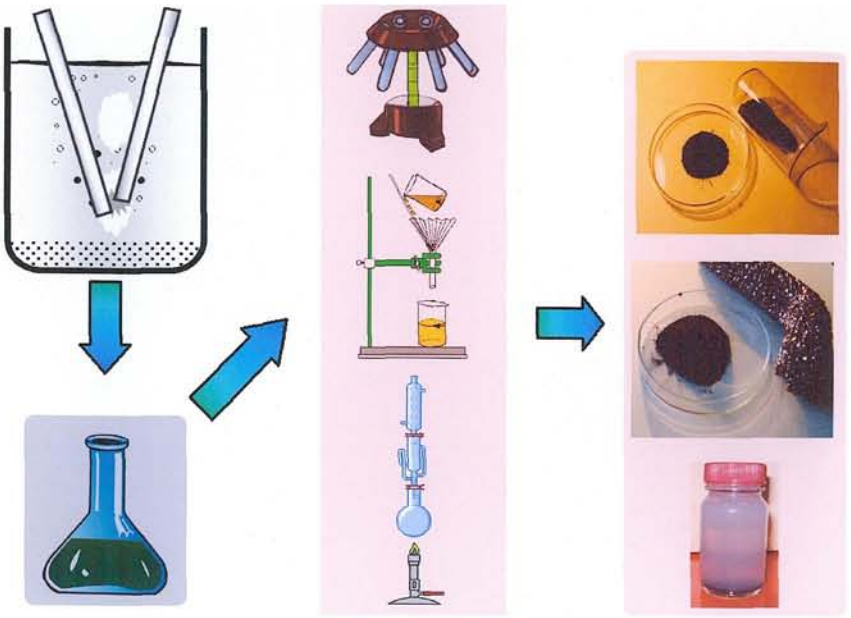

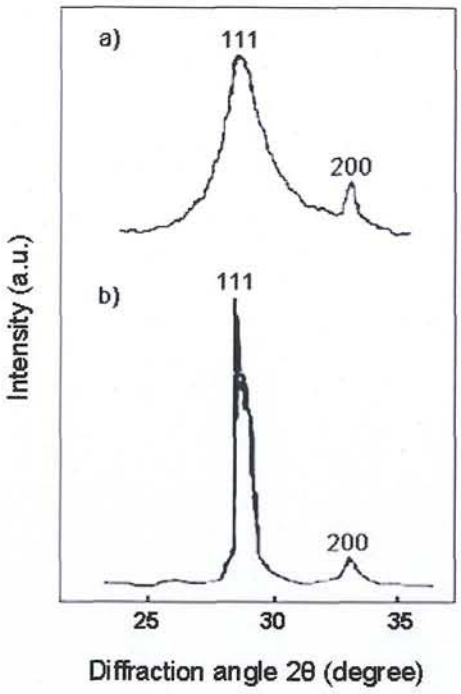

Figure 3-1. Experimental procedure scheme (upper). Below is the XRD pattern for the sample formed by the impulse plasma between ytterbium electrodes in styrene (a) and XRD pattern of the initial bulk ytterbium (b)

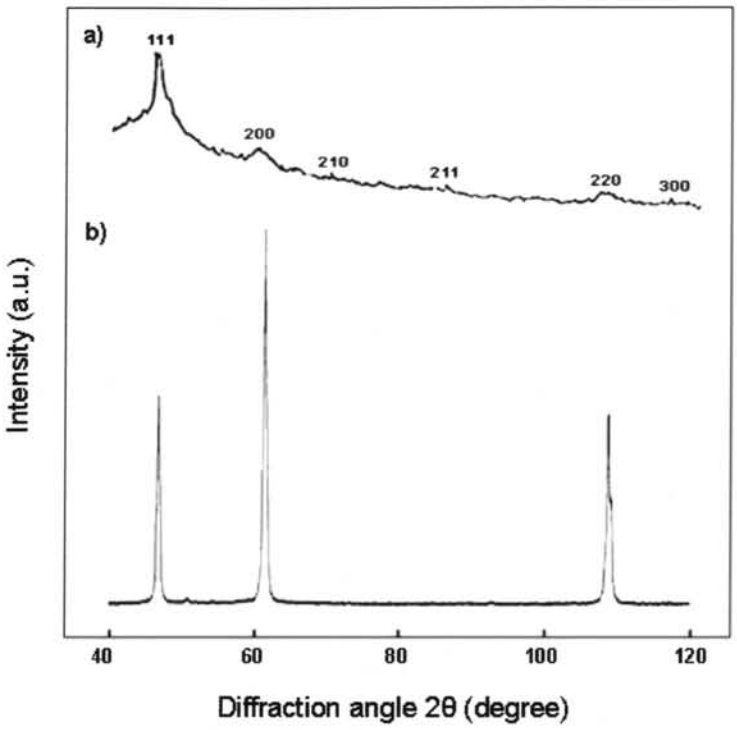

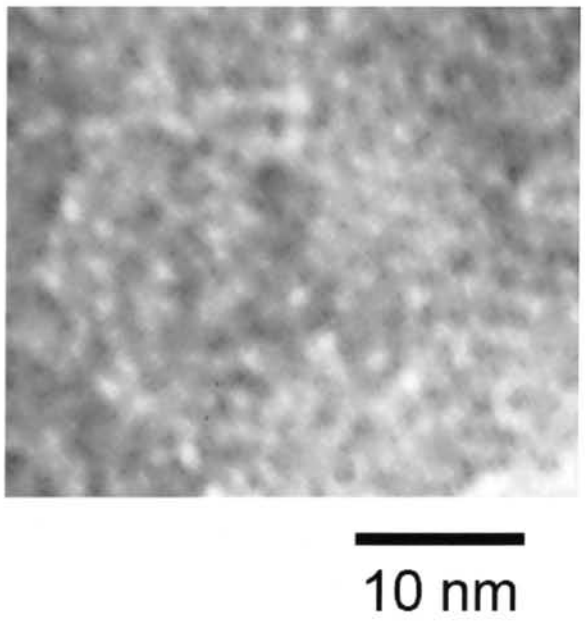

Figure 3-2. a) XRD pattern of the product by the impulse plasma between copper electrodes in styrene and b) XRD pattern of the bulk copper. The bottom figure shows the TEM image of the copper particles by this method

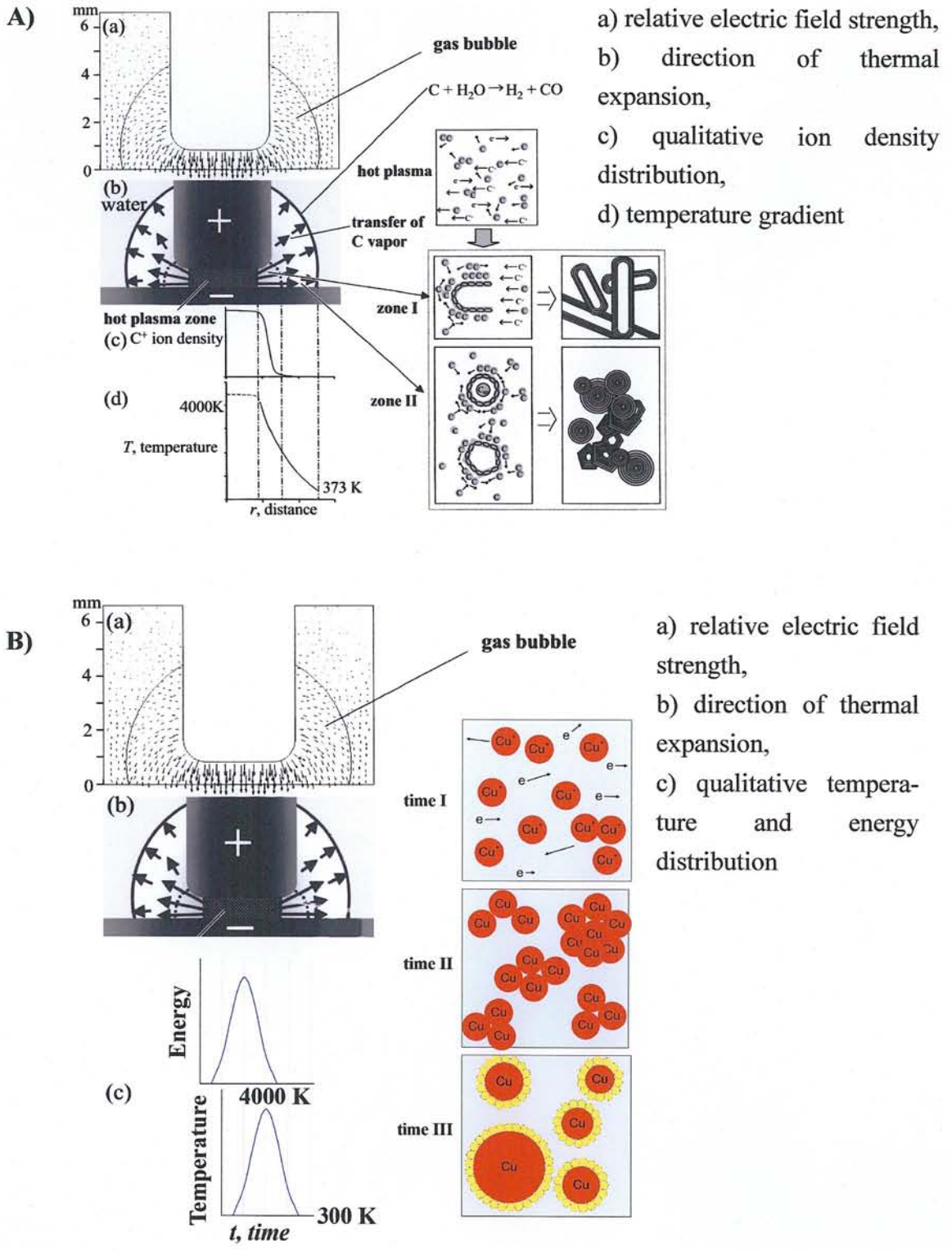

Figure 3-3. Water arc model for the carbon nanomaterials (A) and the nanoparticles formation mechanism by the impulse plasma in liquid method (B)

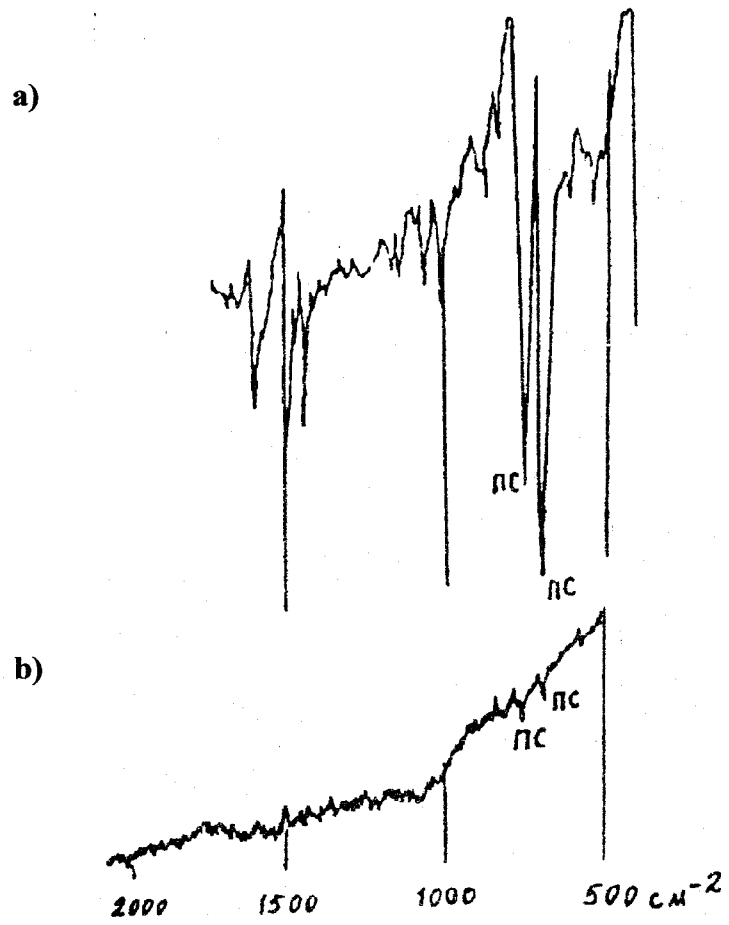

Figure 3-4. a) IR spectra of the separated polymer shell from the copper particles prepared by the impulse plasma between copper electrodes submerged into styrene and b) as-prepared copper particles

Chapter 4
Fullerene C_{60}

4.1 Introduction

C_{60} is a molecule that consists of 60 carbon atoms, arranged as 12 pentagons and 20 hexagons. The shape is the same as that of a soccer ball: the black pieces of leather are the pentagons, the hexagons are white. Depending on the number of hexagons, molecules of different sizes are obtained. They are called fullerenes, after the architect Richard Buckminster Fuller. Fuller, who is shown on the cover of Time Magazine of January 10, 1964, was renowned for his geodesic domes that are based on hexagons and pentagons.

The C_{60} molecule was discovered by Harold Kroto, James Heath, Sean O'Brien, Robert Curl and Richard Smalley in 1985 (Nature 318, 162). The group actually tried to understand the absorption spectra of interstellar dust, which they suspected to be related to some kind of long-chained carbon molecules. Unfortunately they could not solve that problem. But their work was not completely unsuccessful, since in the course of their experiments they discovered the Buckyball which generated so much excitement among scientists and won Curl, Kroto and Smalley the 1996 Nobel prize in chemistry.

The discovery of C_{60} has stimulated a large activity in chemistry. It opened up the new branch of fullerene-chemistry which studies the new families of molecules that are based on fullerenes.

Fullerene C_{60} or buckminsterfullerene [1] was discovered in very small quantities in 1985 by H. W. Kroto (Sussex Univ., UK) and R. E. Smalley (Rice Univ., USA). Things changed dramatically in 1990, when Kratscher and Huffman discovered how to produce pure C_{60} in much larger quantities [2]. This opened up completely new possibilities for experimental investigations and started a period of very intensive research.

Grosser and Hirsch [3] vaporized graphite under similar conditions but in the presence of $(CN)_2$ and obtained a series of dicyanopolyyne products. Since, the arc discharge in gas requires high power and complex cooling and vacuum systems, electrical discharge between graphite electrodes in liquid could be more effective. Therefore, many researchers

tried to synthesize fullerene C_{60} by arc discharge in liquid. Recently, arc discharge methods in liquids have been used for production of metal particles, metal nitrides/carbides/oxides, [4-6] carbon onions [7] and carbon nanotubes [8-10], etc. However, the attempts to synthesize fullerenes by the arc discharge in liquid were not successful [11]. Arc discharge produces continuous plasma, which causes formation of large-size particles. In addition, this method needs high electrical energy and induces rapid evaporation of liquids.

Here we presented a new synthesis method of fullerene C_{60} using impulse plasma in liquid by the low voltage spark discharge [12-14]. The fullerene C_{60} was for the first time synthesized by electric discharge method in liquid. The purity of C_{60} was > 99 %, which is much higher than those by the conventional arc plasma in inert gas methods (less than 80 % C_{60} and 20 % C_{70} and other fullerenes).

4.2 Experimental procedure

Two rods of graphite electrodes (6 mm diameter, 99.97 % purity) were submerged into 150 ml toluene (99.5% purity) and one of them was vibrated within the 0-1 mm gap between their tips. When the circuit was connected to the alternating current (AC) power source (200 V, 0.5 A), impulse plasma was observed between the electrodes in toluene. During the discharge reaction, some of the formed particles were solved by toluene and unsolved particles fell down to the bottom. Obtained toluene solution was sublimated at 110 °C to extract the fullerenes.

XRD patterns of the samples were taken using Cu Kα radiation, Rigaku RINT-2500VHF. The electron microscopy images of the products were taken by Transmission Electron Microscope (TEM) JEOL-200FX: some amount of powder samples were dropped to methanol solution and were ultrasonicated for 3 minutes. Then the particles were collected by copper grids (200 mesh) and were dried in air for TEM observations. Chromatogram and UV-visible spectrum for the extracted fullerene soot and pure C_{60} were taken by the High Performance Liquid Chromatography (HPLC) with the following conditions: MD-2010 Plus, Sil-ODA-14 column, 254 nm, hexane mobile phase, flow rate of 1ml/min, column temperature of 30 ℃.

4.3 Results and discussion

4.3.1 Fullerene C_{60}

The photos of the produced fullerene containing solution by the impulse plasma between two graphite electrodes submerged into toluene and the extracted from this solution fullerene soot are shown in the Figure 4-1.

Figure 4-2 shows chromatogram (a) and UV-visible spectrogram (b) of the sample, produced by impulse plasma using graphite electrodes in toluene and the pure commercial fullerene C_{60}. HPLC analysis of our sample showed two peaks at the retention times 2.23 and 5.16 minutes. The first peak was caused by toluene. The second peak at the retention time of 5.16 min is due to fullerene C_{60}. This was confirmed by the measurement of the commercially available pure C_{60} (dotted line in Fig. 4-2a). The UV-visible spectrum of our sample (at 5.16 min) is in good agreement with the one of pure C_{60} (Fig. 4-2b). Peaks of C_{70} and other fullerenes were not detected. The purity of C_{60} by the present method was estimated to be >99 % by HPLC analysis, which is much larger than those of arc discharge in gas (less than 80 % C_{60} and 20 % C_{70} and other fullerenes).

Figure 4-3 shows TEM images of the fullerene soot produced by the impulse plasma between two graphite electrodes in toluene. We can see a large particle (Fig.4-3a), which was aggregated from very small round shaped particles (Fig.4-3b). Even though the fullerenes cannot be seen clearly from the images due to its very small size (0.7 nm), we can see that it contains of very small round shape particles of less than 10 nm size.

Figure 4-4 represents XRD pattern of the fullerene soot produced by the arc discharge in inert gas and the sample by the impulse plasma between graphite electrodes submerged in toluene (sample collected from the bottom part of the discharge solution). The XRD patterns of the fullerene soot by arc discharge and impulse plasma exhibit almost same peaks, except a wide peak between 10 to 25 degrees in the sample by the impulse plasma. The peaks of the fullerene C_{60} or C_{70} are mainly between the diffraction angles from 10 to 20 degrees. Our sample showed a wide peak between the diffraction angles from 10 to 25 degrees, indicating that the sample contains amorphous structures. So, we can assume that these are the amorphous fullerene particles, which had no time for complete formation due to the short duration of the plasma impulses. However, because of the high solubility of fullerenes in toluene, the completely formed fullerenes were immediately solved by the surrounding toluene leading to the natural purification of C_{60}.

This was confirmed by the HPLC analysis of the particles extracted from the discharge solution (Fig. 4-2), which revealed that the purity of the C_{60} is nearly 99 %.

4.3.2 Effect of the frequency

Effect of frequency on the formation of nanoparticles was also studied. For this purpose, the inverter was adjusted at 60, 600 and 1200 Hz frequency. Figure 4-5 shows the XRD pattern of the sample by impulse plasma in styrene between two iron electrodes with different frequency and the particle size distribution of the samples at different frequencies. We can see that the phase compositions of the samples produced at different frequencies are the same, which means that the frequency (ranging from 60 to the 1200 Hz) did not have any effect to the phase composition of the products. Particles of the bottom and upper parts are mixed and were not separated. This resulted in the large value of the particle size distribution graph. What we paid attention here is the effect of frequency. The bottom graph represents the dynamic light scattering results for the sample produced by the impulse plasma between two iron electrodes submerged into styrene. From the result we can see that the particles sizes increased by increasing the frequency. However, at 1200 Hz, particles size graph showed two peaks of the size distribution. This means that by increasing the frequency above 1200 Hz, small particles formation also increased. Increasing of the small particles formation by increasing the frequency can be associated with the impulse plasma duration.

4.4 Conclusions

In summary, we presented a new method for synthesis of nanomaterials by using impulse plasma in liquid. The fullerene C_{60} was for the first time synthesized by electric discharge in liquid between two graphite electrodes submerged into toluene. The purity of the synthesized fullerene C_{60} was >99 %. This method does not need vacuum system, cooling system, etc., in addition to the low electrical power.

Even though the phase composition of the sample produced at the different frequency remained the same, changing the frequency of the impulse plasma resulted in the increasing the formation of the small sized particles.

References

[1] H. W. Kroto, J. R. Heath, S. C. O'Brien, R. F. Curl, R. E. Smalley, Nature, 1985, 318, 162

[2] Kratschmer, W.; Lamb, L. D.; Fostiropoulos, K.; Huffman D. R. Nature 1990, *347,* 354

[3] Grosser, T.; Hirsch A. Angew. Chem., Int. Ed. Engl. 1993, *32,* 1340

[4] T. Satsuta, M. Hasegawa, N. Harada and S.J. Asai, Jpn. Inst. Metal. 57, 296 (1993)

[5] T. Sato, K. Usuki, A. Okuwaki and Y. Goto, J. Mater. Sci. 27, 3879 (1992)

[6] S.Y. Xie, Z.J. Ma, C.F. Wang, S.C. Lin, Z.Y. Jiang, R.B. Huang and L.S. Zheng, J. Solid State Chem. 177, 3743 (2004)

[7] N. Sano, H. Wang, I. Alexandrou, M. Chhowalla, K.B.K. Teo, G.A.J. Amaratunga and K. Iimura, J. Appl. Phys. 92, 2783 (2002)

[8] Y.L. Hsin, K.C. Hwang, F.-R. Chen and J.-J. Kai, Adv. Mater.13, 830 (2001)

[9] H.W. Zhu, X.S. Li, B. Jiang, C.L. Xu, Y.F. Zhu, D.H. Wu and X.H. Chen, Chem. Phys. Lett. 366, 664 (2002)

[10] H. Lange, M. Sioda, A. Huczko, Y.Q. Zhu, H.W. Kroto and D.R.M. Walton, Carbon 41, 1617 (2003)

[11] F. Cataldo, Carbon 42, 129 (2004)

[12] E. Omurzak, J. Jasnakunov, N. Mairykova, A. Abdykerimova, A. Maatkasymova, S. Sulaimankulova, M. Matsuda, M. Nishida, H. Ihara, T. Mashimo, J. Nanosci. Nanotechnol. 2007, *7,* 3157

[13] E. Omurzak, M. Matsuda, H. Ihara, T. Mashimo, S. Sulaimankulova. Adv.Mater.Res. 15-17 (2007), 549

[14] U.A. Asanov, S.K. Sulaimankulova, J.K. Jasnakunov, E. Omurzak. Chemical Journal of Kazakhstan, 2004, pp. 144-148

Figure 4-1. Photographs of the sample produced by the impulse plasma between two graphite electrodes in toluene (on the left) and the extracted fullerene soot from the liquid (on the right)

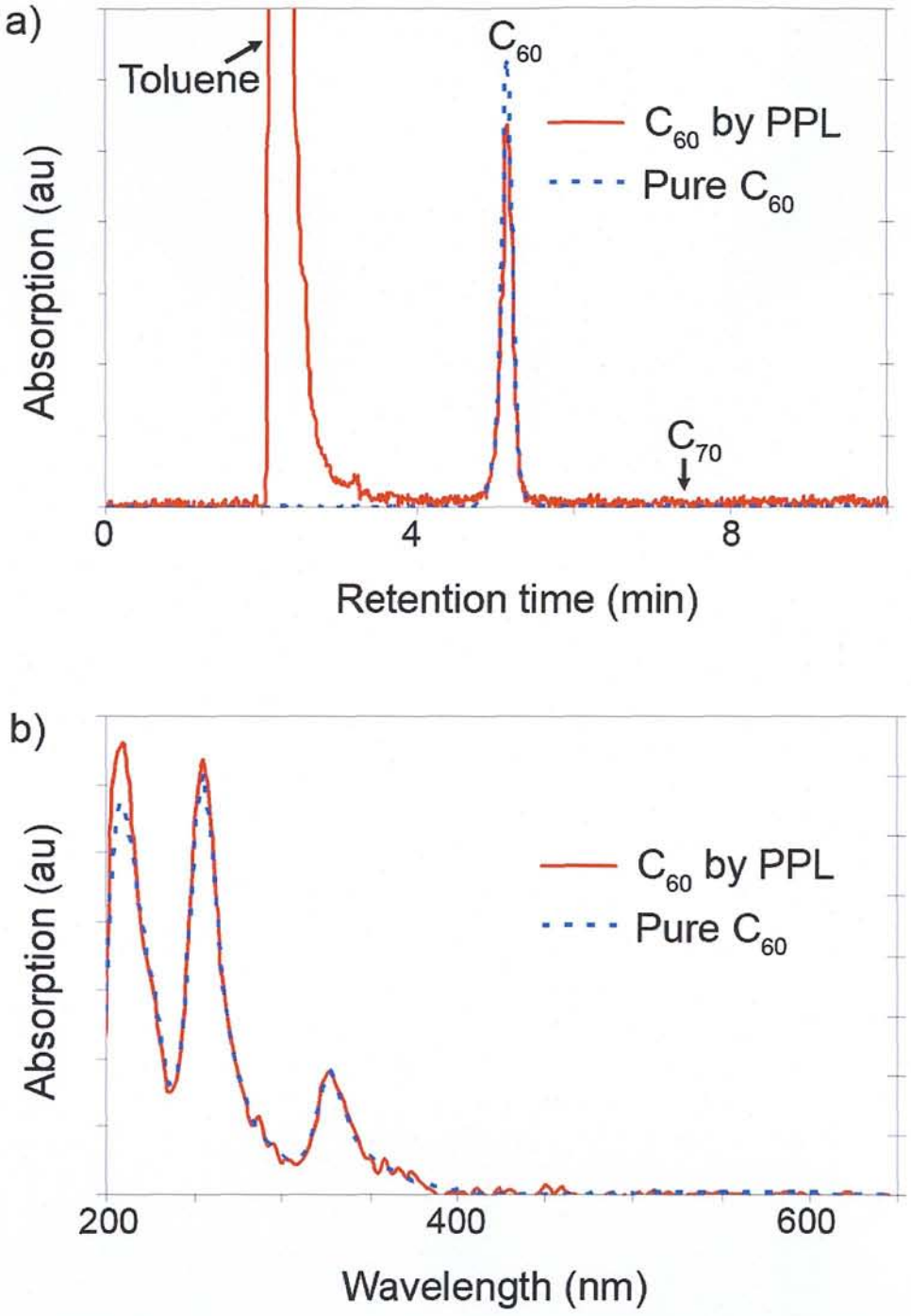

Figure 4-2. a) HPLC chromatogram of the sample produced by the impulse plasma between two graphite electrodes in toluene (red line) and commercial pure C_{60} (dotted blue line), b) UV-Vis spectrum of the samples

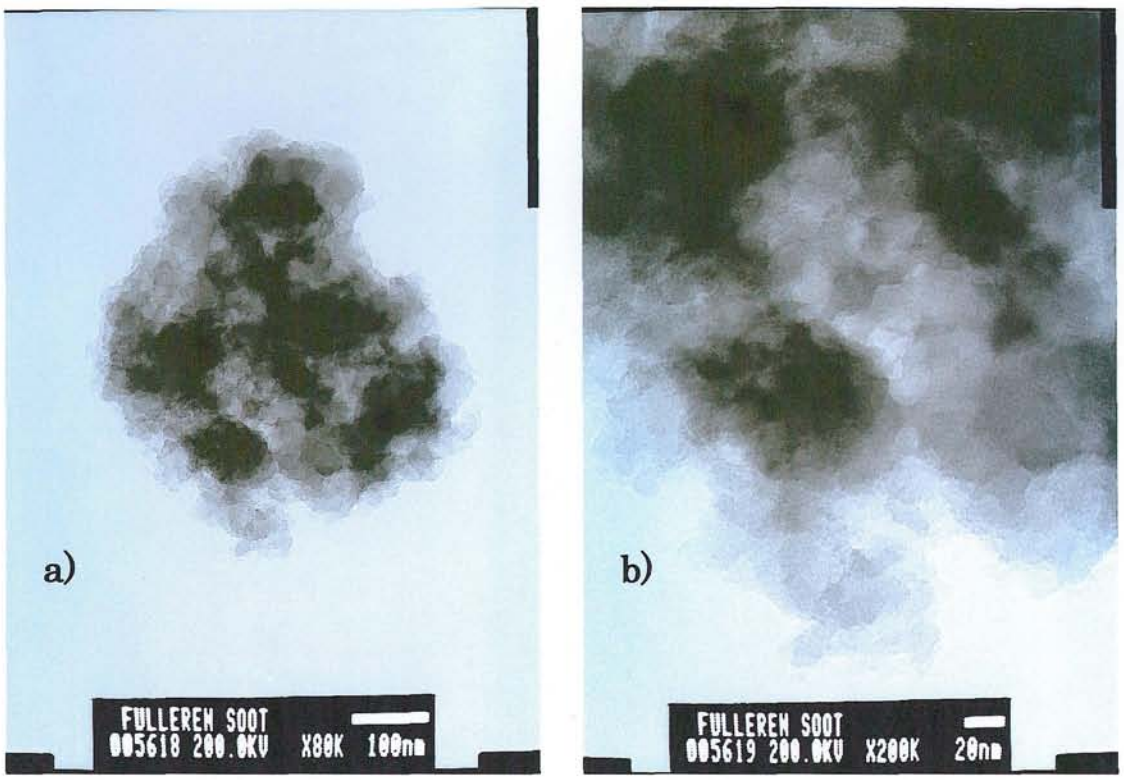

Figure 4-3. a) TEM image of the fullerene soot produced by the impulse plasma between two graphite electrodes submerged in toluene and b) higher magnification image of the particles

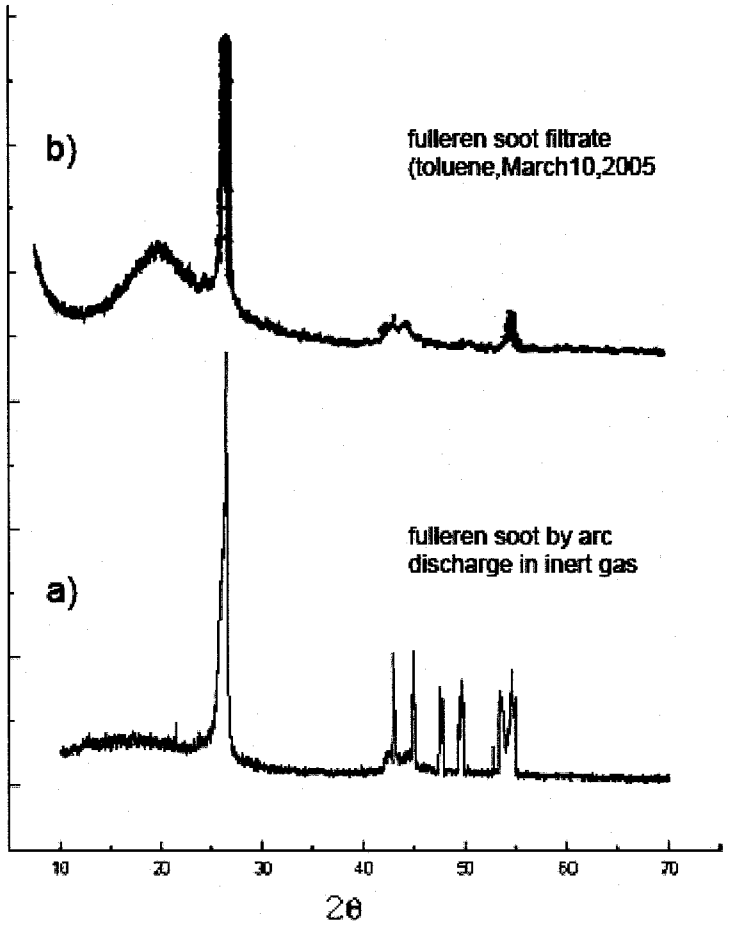

Figure 4-4. a) XRD pattern of the fullerene soot produced by the arc discharge in argon and b) XRD pattern of the fullerene soot produced by the impulse plasma between two graphite electrodes submerged in toluene

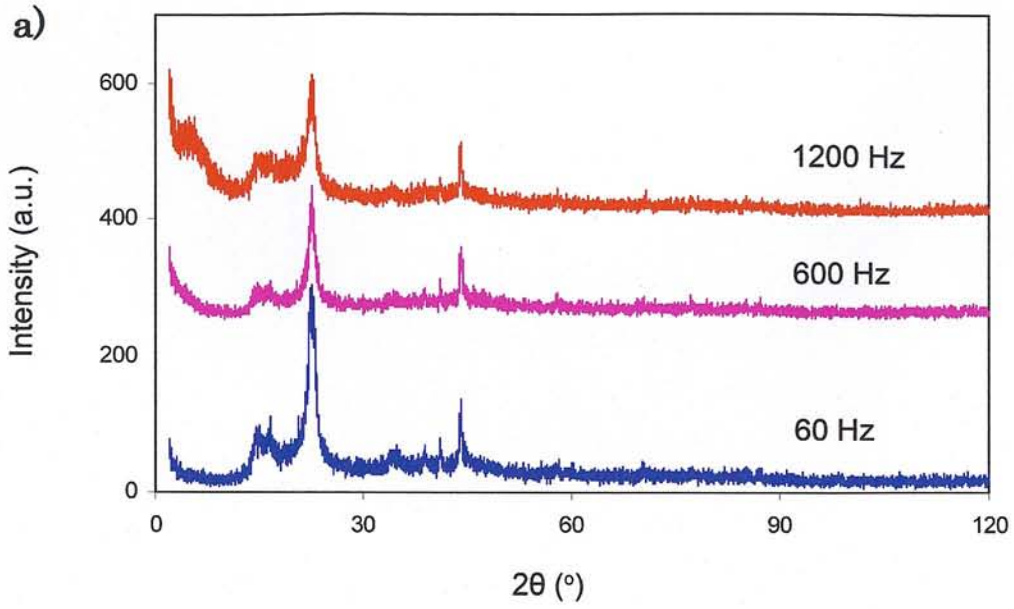

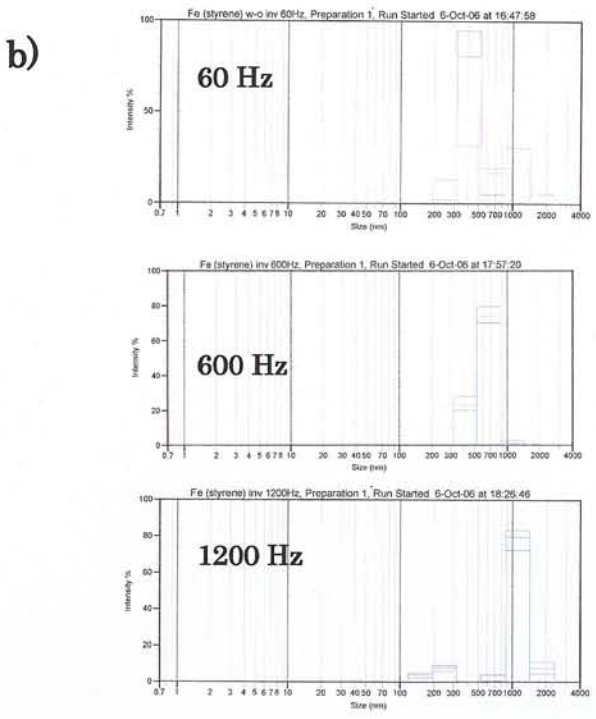

Figure 4-5. a) XRD pattern of the sample by impulse plasma in styrene between two iron electrodes with different frequency and b) particle size distributions of these samples

Chapter 5
Blue anatase TiO_2 nanocrystals

5.1 Introduction

TiO_2 crystallizes in three major different structures: rutile (tetragonal, $a = b = 4.584$ Å, $c = 2.953$ Å), anatase (tetragonal, $a = b = 3.782$ Å, $c = 9.502$ Å) and brookite (rhombohedrical, $a = 5.436$ Å, $b = 9.166$ Å, $c = 5.135$ Å) [1]. Anatase is considered to have higher photocatalytic property than rutile and brookite. Photocatalysis is attributed to the electrical characteristics of TiO_2.

TiO_2 nanoparticles in the 10-50 nm range take on unusual properties and can be used in various applications, such as self-cleaning window glass, air and water purification systems, and antibacterial coating by tapping the photocatalytic properties of these particles. Scientists have adapted them to remove nitrogen oxides from power plant exhausts, and they are looking at ways to harness these environmental catalysts to treat diesel vehicle emissions. TiO_2 is a wide band-gap semiconductor and researchers are looking at it as a substitute for silicon to make solar power cells, as well as battery storage media [2].

According to IUPAC (International Union of Pure and Applied Chemistry) compendium of chemical terminology, photocatalysis is defined as a catalytic reaction involving light absorption by a catalyst or by a substrate [3]. In 1972, Fujishima and Honda discovered the photocatalytic splitting of water on TiO_2 electrodes [4]. Since then, research efforts in understanding the fundamental processes and in enhancing the photocatalytic efficiency of TiO_2 have come from extensive research performed by scientists. In recent years, environmental cleanup applications have been one of the most active areas in heterogeneous photocatalysis. This is inspired by the potential application of TiO_2-based photocatalysts for the total destruction of organic compounds in polluted air and waste waters [5,6]. There are semiconductors which can be used for photocatalysis, such as WO_3, Fe_2O_3, CeO_2, ZnO_2 and ZnS [7]. Metal sulfides are not stable enough for catalysis in aqueous media due to photoanodic corrosion and they are also toxic. Fe oxides undergo

photocathodic corrosion. ZnO is unstable in water and forms $Zn(OH)_2$ on the particle surface [8].

The band gap energy of rutile is 3.0 eV and that of anatase is 3.2 eV. The band gap energies of other photocatalysts are shown in the table 5-1.

The wide band-gap semiconductors can act as sensitizers for light-induced redox processes due to their electronic structure, which is characterized by a filled valence band and an empty conduction band. When a photon with energy of $h\nu$ matches or exceeds the bandgap energy of the semiconductor, an electron is excited from the valence band into the conduction band leaving a hole behind. Excited state conduction-band electrons and valence-band holes can recombine and dissipate as heat. When the aqueous solution of the semiconductor photocatalyst is excited with ultraviolet light, electron-hole pairs develop. These electron-hole pairs have an oxidizing potential of 2.9 V *vs.* normal hydrogen electrode, which is enough to oxidize most pollutants.

Synthesis and physical-chemical properties of the titanium oxides have been extensively studied for the optical, electrical and photocatalytic applications. So far reported synthesis methods such as sol-gel [9-11], chemical deposition [12-13], laser ablation [14,15], magnetic sputtering [16,17], RF glow discharge [18] and vacuum arc discharge [19-21] produce white color powder or transparent thin films of amorphous/anatase/rutile TiO_2 structures. Single crystals of anatase type TiO_2 with a blue color were prepared by chemical transport reaction by using rutile TiO_2 [22]. We developed a new synthesis method for nanomaterials by impulse plasma in liquid [23].

We have synthesized the blue amorphous TiO_2 by the impulse plasma in water.

5.2 Experimental procedure

In this experiment, two electrodes made from 99.9 % purity titanium rods with 6 mm diameter were submerged into 200 ml distilled water in room temperature. Already after several minutes of applying AC electric power (200 V, 3 A), color of water had changed to blue. After about an hour, discharge stopped and the solution was held in a glass for 24 hours in order to let the black particles and blue particles separate naturally by sedimentation of the black ones. Black particles were heavier and fell down to bottom. Then the blue particles were carefully taken for separation by centrifuge. Black particles

were collected form the bottom of the beaker. Formed powders were dried in air at 110 ℃ by muffle furnace.

For the experiments in hot water (60 ℃, 90 ℃), the 200 ml beaker filled with water was placed in a mantle heater for heating. In the case of cold water, the ice bath was prepared in a dish, and then the beaker filled with deionized water was placed inside the ice bath and filled with ice cubes made of pure water. The water temperature was kept at 3 ℃ by adding pure water ice cubes to the discharge water in every 10 minutes.

XRD patterns of the samples were taken using Cu-Kα radiation, Rigaku RINT-2500VHF. The Transmission Electron Microscopy images of the products were taken by Philips Tecnai F20 S-Twin: some amount of discharge solution was taken by pipette and dropped on the copper grids (200 mesh) and were dried at 110 ℃ in air for HRTEM observations. UV-vis spectra of the samples were taken by JASCO V-550 UV/VIS spectrometer. Annealing of the samples was performed in air using electric muffle furnace KM-160.

Photocatalytic properties of the samples were measured using methylene blue (MB) solution decomposition. MB water solution was prepared with 20 ppm concentration. 40 mg of sample is mixed with 20 ml MB solution in a quartz beaker and placed in 12 cm from of the light source (mercury lamp with the central wavelength of 250 nm). After irradiation, the solution was centrifuged (4000 rpm for 15 min). Then the transmittance was analyzed by the spectrometer (UVIDEC-210, wavelength 665 nm). For comparison analysis, the commercially available photocatalytic TiO_2 (ST-01, 95 % anatase) with 7 nm particle size made by the Ishihara Sangyo Kaisha was used.

5.3 Results and discussion

5.3.1 Phase composition of the products

Impulse plasma between the two titanium rods in water had resulted in the formation of two kinds of products, one is the blue suspended particles in water and the second is the black particles at the bottom. Figure 5-1 shows the XRD pattern of the blue particles and a photograph of this sample. From the XRD pattern, we can see that the crystal structure of the sample is amorphous. Figure 5-2a represents the HRTEM image of these blue particles.

Mainly very small particles with diameters of less than 10 nm were observed. Figure 5-2b shows the lattice image of the blue particle showing the nanocrystalline particle with less than 10 nm size. The measured *d*-spacing of the planes from the HRTEM graph is 0.35 nm, matching fairly well with the (101) plane of the anatase TiO_2.

We have also performed the XRD analysis of the black particles collected from the bottom of the solution. Figure 5-3 represent the XRD pattern of the black sample from bottom and its photograph is shown in the Fig. 5-1. Analysis showed that the powder is mainly TiO phase.

5.3.2 Effect of water temperature

In order to examine the effect of water temperature to the formation of the nanoparticles, impulse plasma between titanium rods in different temperature water (3 ℃, 30℃, 60 ℃, 90 ℃) were performed. Here also we got two kinds of products: 1) blue particles suspended in water and 2) black powder sank to the bottom. Figure 5-4 shows the XRD pattern of the blue particles synthesized by the impulse plasma in different temperature water, indicating that the crystallinity of the blue powder increases with increasing the temperature of water. But the phase composition and the color of the formed particles did not change in all the cases. By increasing the water temperature above the boiling point by using for example, autoclave, we expect to obtain higher content of the anatase structure.

5.3.3 Thermal treatment of the blue TiO_2

The blue nanopowder prepared in room temperature water was annealed in air at 300 ℃, 400 ℃, 500 ℃ and 800 ℃ for 3 hours in each annealing temperature. Figure 5-5 shows the XRD patterns of the annealed samples at different temperatures. The blue powder showed amorphous structure without annealing. After the annealing of the blue powder at 300 ℃, the XRD peaks of anatase structure appeared. Already after annealing the sample at 400 ℃ the peaks of the rutile structure appeared. The formation temperature of the rutile is usually above 800 ℃. The formation of the rutile already at 400 ℃ might be due to the energy saturation of the forming particles. Depending on the location from the discharge channel, the forming particles were energy-saturated differently. So, more saturated particles transfer to the rutile structure just after a small heating. After annealing the sample at 800 ℃, it was completely transformed into rutile structure (Figure 5-5). The

blue TiO_2 was stable up to the temperature of 400 °C. So, the color of the samples remained blue after annealing up to 400 °C and it turned gray after 500 °C annealing.

5.3.4 UV-vis absorption spectra

Figure 5-6 shows the UV-Vis absorption spectra of as-prepared blue amorphous TiO_2, annealed blue TiO_2 and the ST-01 samples. The blue amorphous TiO_2 nanopowder showed the highest absorption in the visible light range (400 – 800 nm) than the other samples. Annealing of the blue amorphous TiO_2 caused decreasing of the absorption. Annealed sample at 800 °C, which completely changed to the rutile structure, showed similar UV-vis absorption spectrum with the common rutile phase.

During the formation of the nanoparticles, the impulse plasma in liquid creates many crystallographic defects that give rise to the formation of the color centers. These color centers are considered to be the source for the absorption features displayed by the TiO_2 specimens in the visible spectral region, [24] which possesses 45% of the energy in the solar radiation while the UV light less than 10%. It is expected that the blue amorphous TiO_2 exhibit excellent photocatalytic property in the visible light region.

Thermal treatment of the blue TiO_2 at 300 °C and 400 °C did not cause any significant change in color. However, the sample annealed at 500 °C turned to yellowish color. This also can be seen from the UV-vis absorption spectra: a broad band from 400 nm up to 800 nm exist for the samples up to 400 °C and almost disappear after the annealing at 500 °C. Annealing of the blue TiO_2 at 800 °C caused the formation of rutile structure and consequently the color changed to white. Sekiya et al. [22] reported that the blue color of the anatase crystal is due to the free carrier absorption. And Straumanis et al. [25] showed that depending on the atomic ratio of oxygen and titanium, rutile powder changes from yellowish white to bluish black color.

5.3.5 Photocatalytic property under UV light

Figure 5-7 shows the decomposition of methylene blue solution under UV irradiation. Blue amorphous nanopowder showed lower photocatalytic activity than the ST-01 sample. But, after annealing the sample, the photocatalytic activity increased. Photocatalytic property of ST-01 sample was higher than the annealed samples up to 30 minutes of irradiation (Figure 5-7a). However, after 30 minutes of irradiation, the commercial anatase and the annealed samples showed almost the same decomposition rates (~ 100 %) and it

was not possible to distinguish between them. So, we did the same experiment with the longer distance from the UV light source, this time the distance was 20 cm. After 30 minutes of irradiation, the annealed blue nanopowder showed higher photocatalytic activity than ST-01 sample (Figure 5-7b).

5.4 Conclusions

In summary, the blue colored anatase TiO_2 nanocrystals (less than 10 nm) were synthesized using impulse plasma in liquid method. This sample was stable up to the temperature of 400 ℃. By increasing the temperature of discharge water, the crystallinity of the blue nanopowder increased. Annealing of the blue amorphous TiO_2 at 300-400 ℃ resulted in the formation of blue anatase TiO_2. The blue TiO_2 obtained by this method showed higher absorbance in the visible light than the commercial photocatalyst ST-01. Photocatalytic property of the annealed at 400 ℃ under the UV light was higher than the commercial photocatalyst ST-01.

We expect that the present TiO_2 has high catalytic performance under the visible light for applications such as decomposition of pollutants and solar battery electrodes, etc. We are now under the study of analysis of catalytic property, photoluminescence, etc.

References

[1] U. Diebold. Surface Science Reports 48 (2003), 53

[2] M. S. Reisch. Chemical & Engineering News 81 (2003), 13

[3] J. W. Verhoeven. Pure and Applied Chemistry 68 (1996), 2223

[4] A. Fujishima, K. Honda. Nature 238 (1972), 37

[5] A. Fujishima, T. N. Rao, D. A. Tryk. Journal of Photochemistry and Photobiology C: Photochemistry Reviews 1 (2000), 1

[6] D. A. Tryk, A. Fujishima, K. Honda. Electrochimica Acta 45 (2000), 2363

[7] K. W. Böer, Survey of Semiconductor Physics, Van Nostrand Reinhold: New York, 1990

[8] M. A. Fox, M. T. Dulay. Chemical Reviews 93 (1993), 341

[9] B.E. Yoldas, J. Mat. Sci. 1986, 21, 1087

[10] M. Zaharescu, M. Crizan, I. Musevic, J. Sol-Gel Sci. Technol. 1998, 13, 769

[11] I. Manzini, G. Antonioli, D. Bersani, P.P. Lottici, G. Gnappi, A. Montereno, J. Non-Cryst. Solids 1995, 192/193, 519

[12] V. Pore, A. Rahtu, M. Leskela, M. Ritala, T. Sajavaara, J. Keinonen, Chem. Vap. Deposition 2004, 10, 143

[13] Y. Gao, Y. Masuda, K. Koumoto, Langmuir 2004, 20, 3188

[14] Harano, K. Shimada, T. Okubo, M. Sadakata, J. Nanoparticle. Res. 2002, 4, 215

[15] C.H. Liang, Y. Shimizu, T. Sasaki, N. Koshizaki, Appl. Phys. A 2005, 80, 819

[16] P. Zeman, S. Takabayashi, Thin Solid Films 2003, 433, 57

[17] D. Depla, S. Heirwegh, S. Mahieu, J. Haemers, R. De Gryse, J. Appl. Phys. 2007, 101, 013301

[18] L.M. Williams, D.W. Hess, J. Vac. Sci. Technol. A 1983, 1, 1810

[19] Z. W. Zhao, B. K. Tay, J. Appl. Phys. 2007, 101, 013505

[20] C. S. Jwo, D. C. Tien, T. P. Teng, H. Chang, T. T. Tsung, C. Y. Liao, C. H. Lin, Rev. Adv. Mater. Sci. 2005, 10, 283

[21] H. Takikawa, T. Sasaoka, Tateki Sasakibara, Electr. Eng. Jpn. 1999, 126, 12

[22] T. Sekiya, K. Ichimura, M. Igarashi, S. Kurita, J. Phys. Chem. Solids 2000, 61, 1237

[23] E. Omurzak, J. Jasnakunov, N. Mairykova, A. Abdykerimova, A. Maatkasymova, S. Sulaimankulova, M. Matsuda, M. Nishida, H. Ihara, T. Mashimo, J. Nanosci. Nanotechnol. 2007, 7, 3157

[24] V.N. Kuznetsov, N. Serpone. J. Phys. Chem. B 2006, 110, 25203
[25] M.E. Straumanis, T. Ejima, W.J. James, Acta Cryst. 1961, 14, 493

Table 5-1. Bandgap energy of various photocatalysts

Photocatalyst	Band gap (eV)
Si	1.1
WSe_2	1.2
Fe_2O_3	2.2
CdS	2.4
WO_3	2.7
TiO_2 (rutile)	3.0
α-Fe_2O_3	3.1
TiO_2 (anatase)	3.2
ZnO	3.2
$SrTiO_3$	3.4
SnO_2	3.5
ZnS	3.7

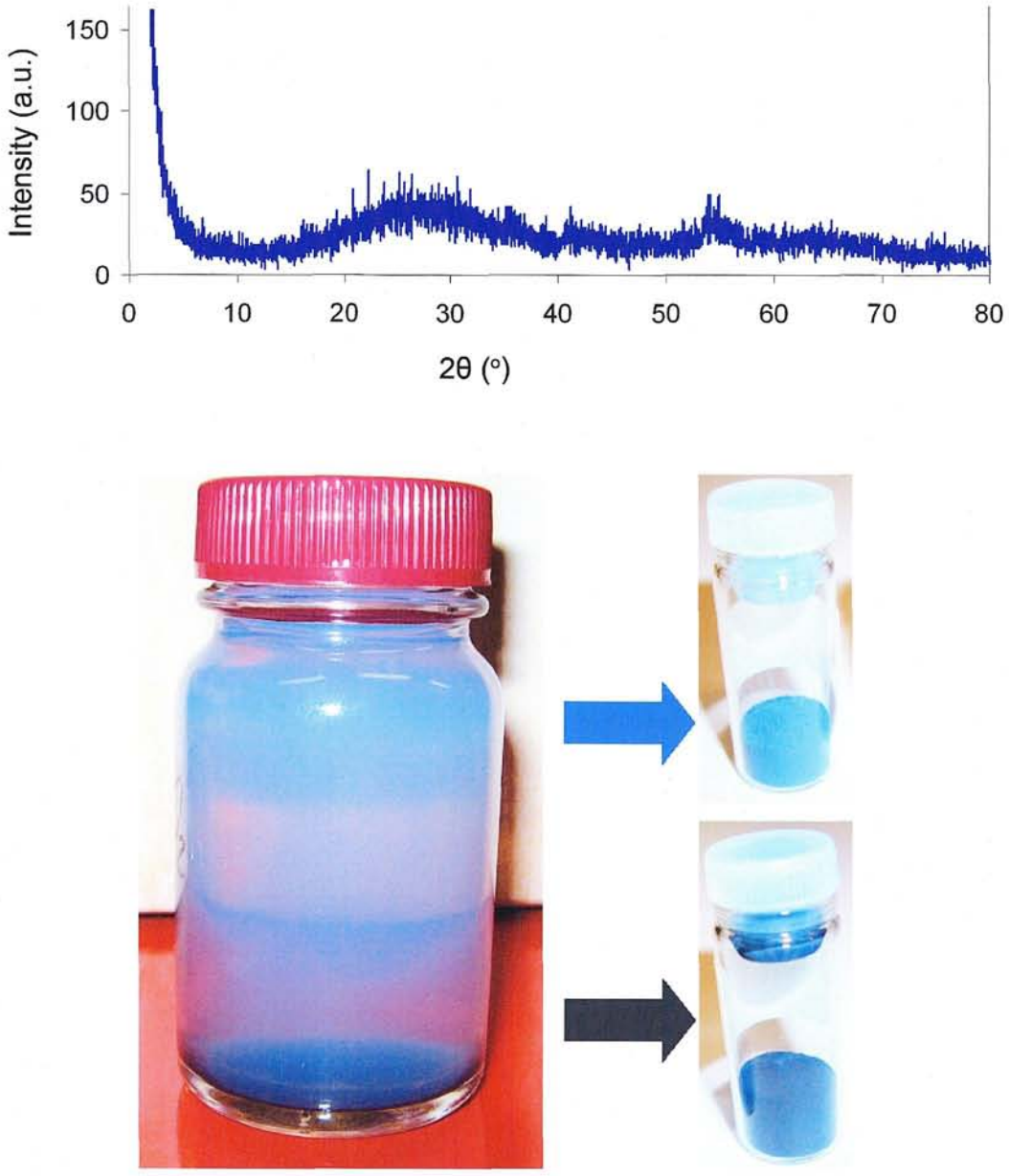

Figure 5-1. XRD pattern of the blue particles (suspended in solution) produced by the impulse plasma (200 V, 3 A) between two titanium rod electrodes submerged in water. At the bottom, photograph of the blue liquid solution and the blue and black powders separated from the solution and collected from bottom, respectively

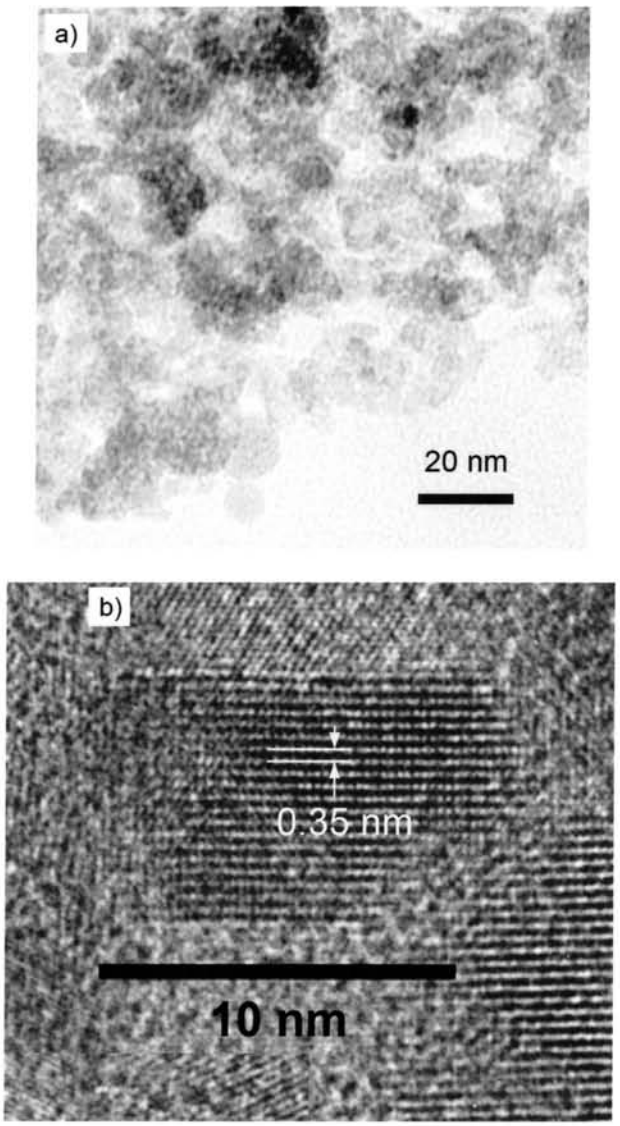

Figure 5-2. a) TEM image of the blue particles and b) lattice image of a single blue particle

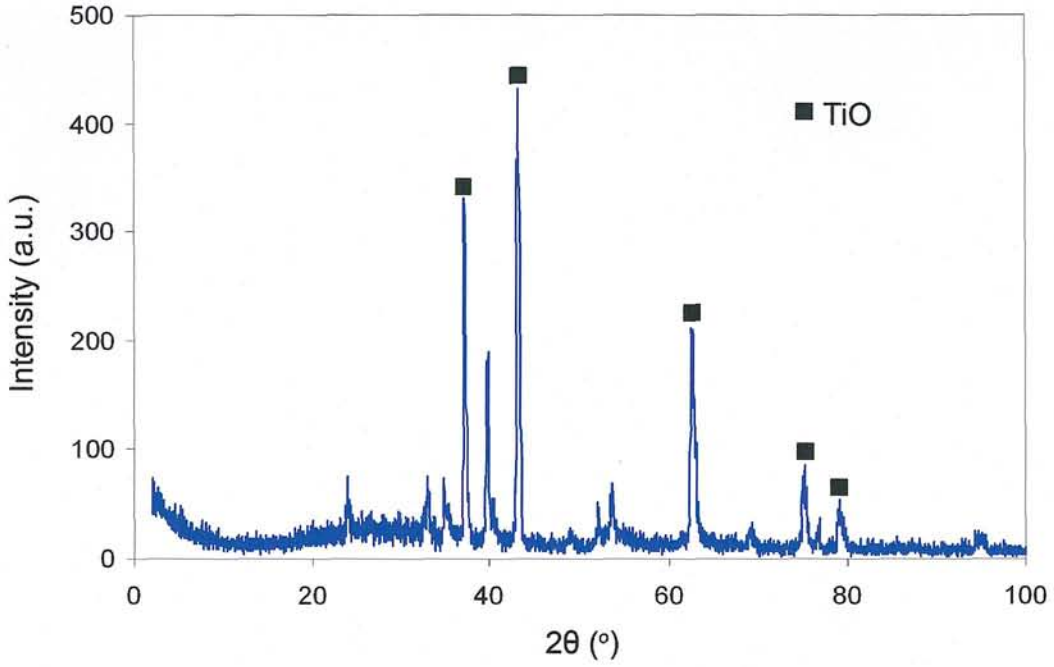

Figure 5-3 XRD pattern of the black particles (collected from the bottom of the solution)

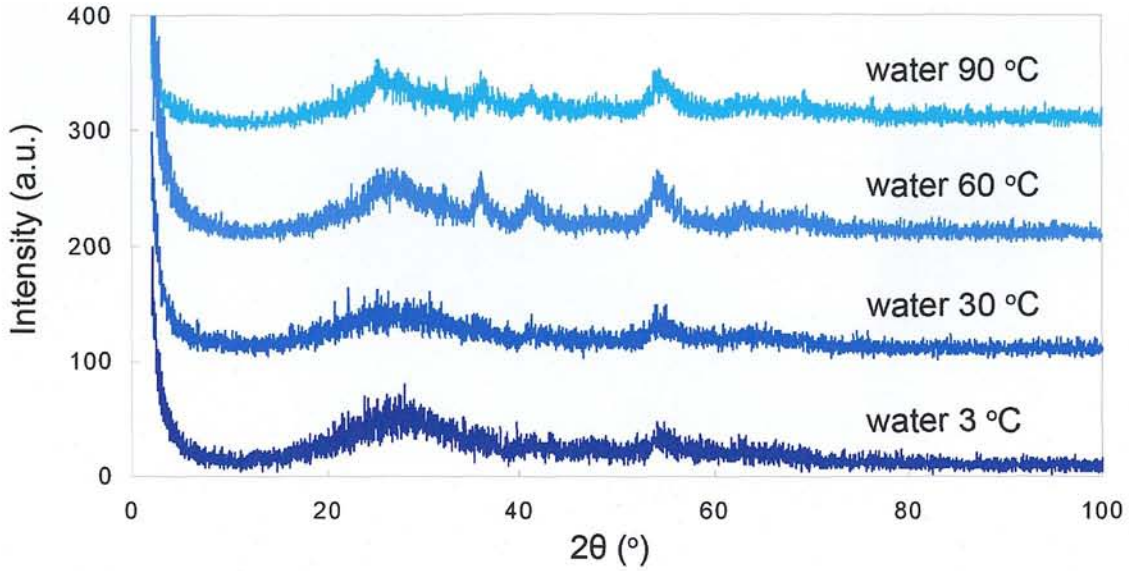

Figure 5-4. XRD patterns of the blue powders, produced by the impulse plasma between two titanium rod electrodes submerged in different temperatures water

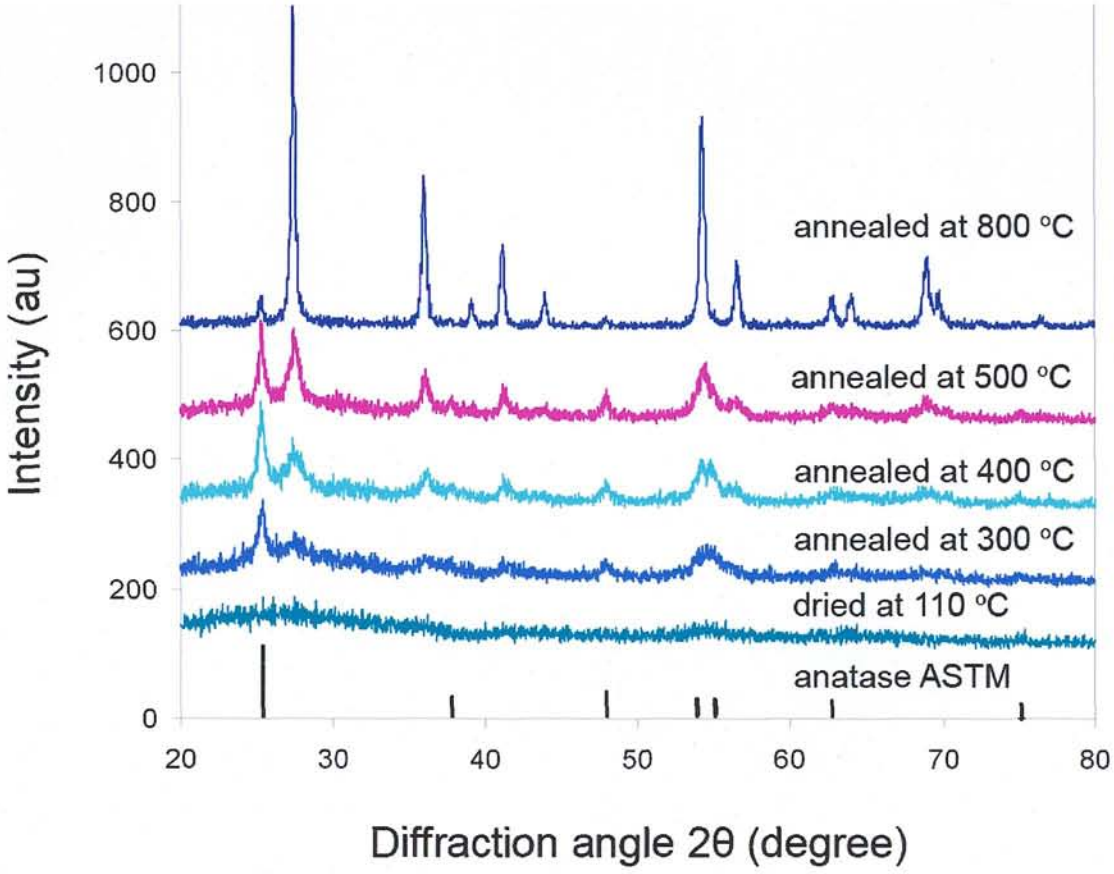

Figure 5-5. XRD patterns of the blue powder after annealing at different temperatures

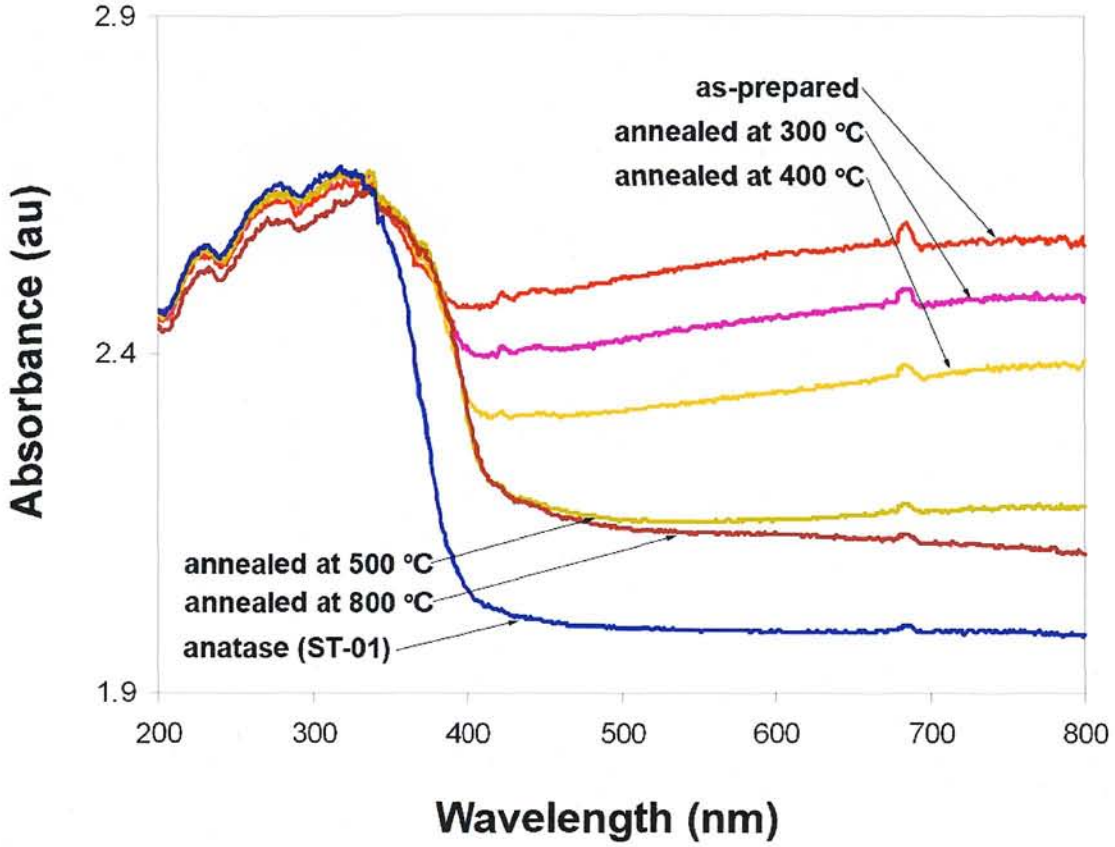

Figure 5-6. UV-Vis absorption spectra of as-prepared, annealed and the ST-01 samples

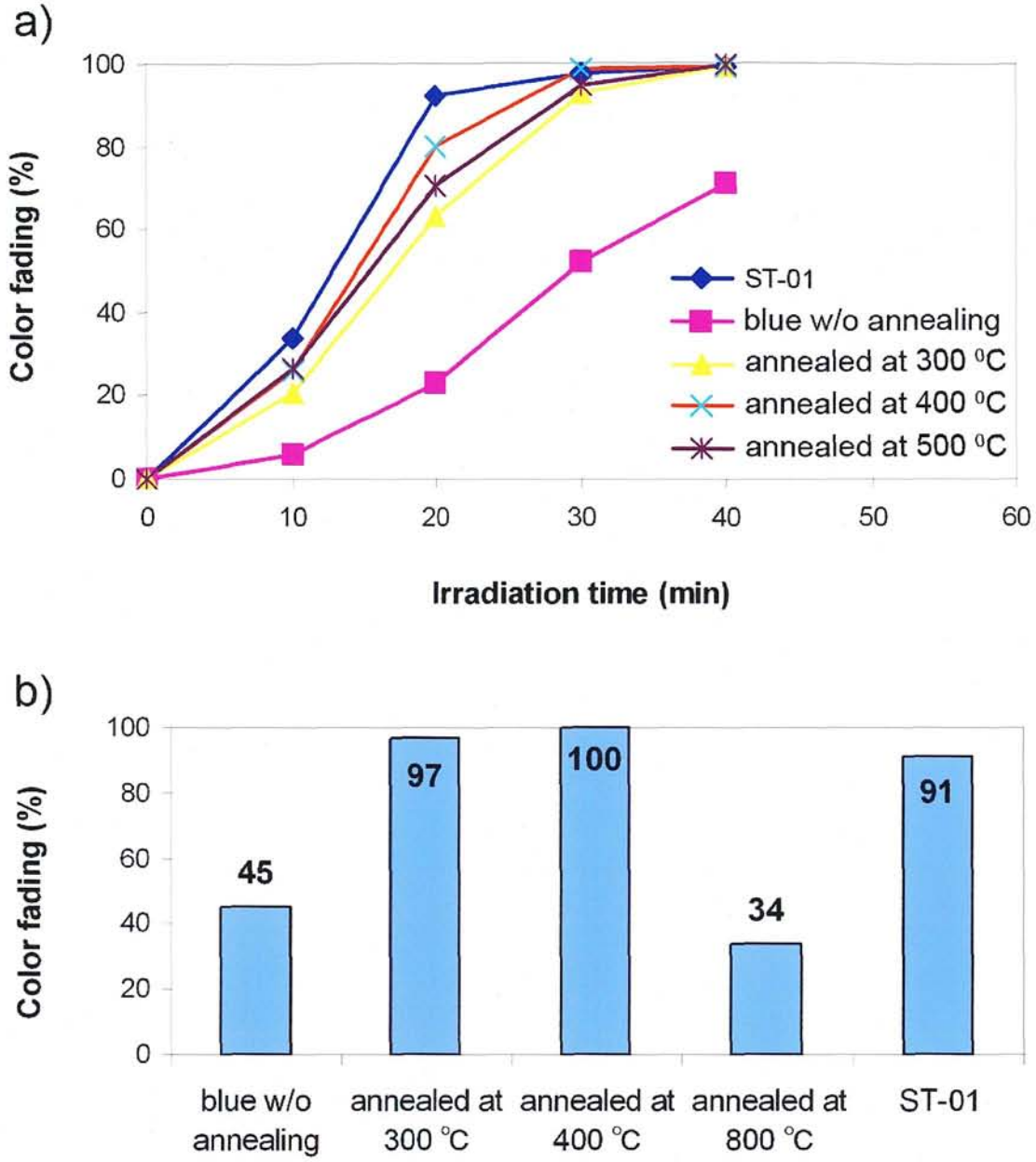

Figure 5-7. a) Decomposition of methylene blue solution by the different samples under the UV irradiation from a distance 12 cm and b) 20 cm for 30 min

Chapter 6
Wurtzite ZnS nanoparticles

6.1 Introduction

6.1.1 II-VI Wurtzite semiconductors

Most of the II-VI semiconductors can form, with some degree of stability in bulk, the wurtzite crystal structure. This crystal structure offers several benefits to the formation and the physical properties of nanomaterials. Generally recognized eight II-VI semiconductor materials are ZnO, ZnS, ZnSe, ZnTe, CdO, CdS, CdSe, and CdTe. Mercury, the other group IIB metal, forms a liquid at standard temperature and pressure and therefore is not generally included in this list. Because of their uses in optoelectronic and semiconducting applications, II-VI semiconductors have recently been the focus of intense research in nanomaterials. The II-VI semiconductors are typically wide band gap materials, serving as efficient light emitters. This makes them likely candidates to replace materials such as GaN in light emitting diodes (LED) [1]. Each of the II-VI semiconductors demonstrate some unique properties, making them useful for unique applications. ZnS has a band gap of 3.54 eV for the zinc blende phase and 3.91 eV for the wurtzite phase [2]. It displays a high refractive index of 2.2 and a high transmittance of light in the visible region of the spectrum [3-5]. These properties make ZnS a strong candidate for optoelectronic devices. So, we focused on ZnS.

Wurtzite ZnS is a direct wide band gap (3.91 eV) semiconductor that is one of the most important materials in photonics. This is because of its high transmittance in the visible range and its high index of refraction (about 2.2). ZnS has been synthesized as nanowires, nanobelts, nanocombs, and, most recently, nanohelices [6-9]. All of these are one-dimensional nanostructures. Recently, ZnS nanobelts have been doped with manganese without changing their crystallography [10]. ZnS doped with manganese (Mn) exhibits attractive light-emitting properties with increased optically active sites for applications as efficient phosphors. Furthermore, single ZnS nanobelts have been shown to

facilitate optically pumped lasing [11]. All of these properties make ZnS nanostructures attractive candidates for use in devices and other technologies.

ZnS is also an important phosphor host lattice material used in electroluminescent devices (ELD), because of the band gap large enough to emit visible light without absorption and the efficient transport of high energy electrons.

Zinc sulfide has two types of crystal structures: hexagonal wurtzite ZnS (referred to as "hexagonal phase") and cubic zinc blend ZnS (referred to as "cubic phase"). Typically, the stable structure at room temperature is zinc blend, with few observances of stable wurtzite ZnS.

Wurtzite is the most stable structure for CdS and CdSe and the other II-VI semiconductors have previously been observed to exhibit the wurtzite crystal structure when synthesized under the right conditions [12-14].

6.1.2 Electroluminescent display

Zinc sulfide is an important phosphor host material, used in thin film, electroluminescent displays, and many other phosphor applications. A typical electroluminescent display device consists of a very basic structure. There are at least six layers to the device. The first layer is a base plate and it is usually a rigid insulator like glass. The second layer is a conductor. The third layer is an insulator. The fourth layer is the phosphor material. The fifth layer is an insulator. Finally, the sixth layer is another conductor. Of course, at least one of the conductors must be transparent so that the light can escape the device. Essentially, ELDs are somewhat “lossy” capacitors that becomes electrically charged like a capacitor and then loses its energy in the form of light. The insulator layers are necessary to prevent arcing between the two conductive layers.

In summary, this thesis will focus on one-dimensional ZnS nanomaterials, their synthesis, and properties. The review above provides the framework for this exploration and the motivation behind it.

6.1.3 Synthesis of ZnS

Considerable efforts recently have been made to synthesis nanostructures of ZnS materials and study of their physical properties. So far, several approaches, such as vapor-phase growth method [15], laser assisted catalytic [16,17] and thermal evaporation [18-20], have been reported for the preparation of ZnS. However, ZnS nanostructures synthesized

by previously reported solution methods were usually zinc blend, which is a low-temperature phase. In practical applications, wurtzite ZnS is often needed. To synthesize single crystalline wurtzite ZnS nanostructures, it is required to use expensive instruments and perform experiments at high temperature. In addition, it is important to synthesis nanostructure of ZnS with crystallographic defects (stacking faults), which are concerned to be the significant feature for the photoluminescence.

Here we present a new catalyst-free, low-temperature method for the synthesis of the wurtzite ZnS by the impulse plasma in liquid.

6.1.4 Features of shock compression

Shock compression of solids has some different features from static compression: pulsed short duration less than microsecond, uniaxial compression, heterogeneous state, etc. Dynamic consolidation by shock compression has considerable potential for high relative density metastable materials or high strength materials which are very difficult to sinter by conventional techniques. Formation of dense compacts requires the collapse of the gaps between the particles as well as considerable amount of energy deposited at the particle surfaces for interparticle bonding. The ultra rapid deformation and energy deposition in shock consolidation produces partial melting at the particle surfaces followed by a rapid solidification via heat conduction into the interior of the particles [21]. The increase of the temperature in the interior of the particles is quite limited because the duration time of shock pressure is quite short. Therefore, shock compression can be used as an effective consolidation method for metastable material powders without recrystallization or decomposition.

6.2 Experimental procedure

6.2.1 Synthesis of ZnS

ZnS nanostructures were prepared using the impulse plasma in liquid method [22]. Rod electrodes with diameters of 10 mm made from 99.9 % purity zinc were fixed in the form of V. One of the electrodes was vibrated with about 3 mm amplitude in order to keep the impulse plasma process stable. A 200 ml pyrex beaker filled with 99.5 % purity sulfur powder was placed on the mantle heater. The sulfur was heated 140 ℃ to be melt and was

kept at this temperature throughout the experiment. The beaker was placed inside the fume hood to prevent the toxic air from the sulfur. The electrodes were submerged into the molten sulfur and the power (200 V, 3 A) was applied. After 30 minutes, the impulse plasma was stopped and the solution temperature was cooled down naturally. The obtained powder was crushed and then washed by the boiling xylene in order to purify the sample from the sulfur.

XRD patterns of the samples were taken using Cu-Kα radiation, Rigaku RINT-2500VHF. Scanning Electron Microscope image were taken using JSM-5310LV. The Transmission Electron Microscopy images of the products were taken by Philips Tecnai F20 S-Twin: some amount of discharge solution was taken by pipette and dropped on the copper grids (200 mesh) and were dried at 110 ℃ in air for HRTEM observations.

6.2.2 Shock compression

For comparison with ZnS by the impulse plasma, commercial ZnS sample was used. ZnMgS (Cu doped) powder was prepared by adding Cu_2S, MgS and NaCl to ZnS and annealing at 1000 ℃ under the argon atmosphere. After that, the sample was inserted into the iron capsule for carrying out the shock compression experiments. Shock recovery experiments were conducted by using keyed-powder gun.

T. Mashimo et al. had developed the keyed-powder gun (1SKG-KM1) of 27 mm in bore diameter for impact-shock study of solids in several 10s GPa region [23]. Figure 6-1a shows the photograph of the keyed-powder gun. This gun was capable of accelerating a projectile to a velocity of over 2 km/s without rotation due to the tenacious keyed launcher, and generating the combined compression-shear shock waves as well as normal shock wave of several 10s GPa. Figure 6-1b shows the sketch map of the assembly used in the shock compression recovery experiments.

The thickness of the sample inserted into the capsule was 2 mm. Impacting plates made of 1 mm thickness tungsten and 2 mm copper plates were used for the shock compaction at the shock velocity of 0.7km/s~1.2km/s. The capsule used by this research was 12 mm inside diameter. Impact plate was attached to the front of projectile so that it hits the sample containing capsule when the gun is launched. The experimental and the sample conditions are summarized in the table 6-1.

6.3 Results and discussion

6.3.1 Wurtzite ZnS by the impulse plasma

Figure 6-2 represents the XRD pattern of the sample produced by the impulse plasma between two zinc electrodes in sulfur. We can see that the sample consists of ZnS wurtzite structure and metallic Zn. As the destructibility of zinc by impulse plasma is high, amorphous content is negligibly small. However, percentage the metallic particles, which did not react with sulfur is high. Natural separation of ZnS from Zn by sinking of heavier Zn does not work. Because, sulfur needs to be heated in order to be in the liquid form. During the heating, the natural sedimentation of the heavier particles does not occur. That is one of the reasons why the reflections of the metallic particles in the XRD pattern remained large. The content of the metallic particles of Zn can be reduced by:

1. adjusting impulse duration, energy, etc for proper reaction time
2. solving of zinc particles with acid or other solvent and separate the ZnS,
3. separation by melting of Zn, since the melting temperature of Zn is 420 ℃ while the melting point of ZnS is over 1700 ℃.

Figure 6-3a shows the lattice image of a ZnS crystal by the impulse plasma between two zinc electrodes in sulfur. The arrows denote the stacking faults in the ZnS crystal with 5 nm size. Figure 6-3b shows the HRTEM image of a bigger sized ZnS crystal with stacking faults denoted by arrows. So the stacking faults were also found in the bigger particles of ZnS (50 nm). Figure 6-4 represents the HRTEM Energy Dispersive X-Ray spectrum (EDX) of the particle with the stacking faults. EDX spectrum revealed the peaks of Zn, S, C, Cu and a small amount of oxygen. The source of the carbon and the copper is the microgrid that was used as the sample holder for TEM analysis, because, the microgrid is made of copper and coated with the carbon mesh. The EDX spectrum quantification results can be seen in the Fig. 6-4b. From this result we can conclude that the particle with the stacking faults is ZnS.

The rapid quenching from the high temperature plasma state and non-equilibrium conditions of the impulse plasma here also played an important role in the creation of the metastable wurtzite phase of ZnS.

6.3.2 ZnS/MgS by the impulse plasma

Figure 6-5a shows the XRD pattern of the sample by the impulse plasma between magnesium and zinc rods in sulfur. The reflections of the wurtzite structure ZnS were identified. Magnesium sulfide was also revealed. The content of the metallic zinc still remained significant. However, due to the lower destructibility of the magnesium, the metallic particles of magnesium were not revealed. So we can say that the existence of the metallic particles of zinc is probably due to the higher destructibility of zinc electrode by the impulse plasma than the magnesium.

Figure 6-5b represents the TEM image of the sample produced by the impulse plasma between Zn and Mg electrodes in sulfur. As we can see, the particles are spherically shaped and the size of the particle is between few nanometers and up to 50 nm. The stacking faults can be seen in a number of particles.

This experiment was performed in order to examine possibility of the impulse plasma in liquid for doping of ZnS with other metals such as Mg, Cu, Mn, etc. So, from these results we can say that the doping of ZnS is possible by the impulse plasma. In addition, by this method we can combine several processes (synthesis, creating crystal defects, doping, etc) in one.

6.3.3 Effect of shock compression on ZnMgS

Figure 6-6 shows TEM images indicating the crystal condition of the ZnMgS before the shock treatment. The particles are clear and there are no crystallographic defects. TEM analysis of the sample treated by the shock wave at the impact velocity of 0.68 km/s did not show any significant change of the crystal state. However, powders treated by the shock wave with the impact velocity at 1.0 km/s and 0.91 km/s were successfully compacted and were hard enough. ZnMgS powder was successfully compacted at the impact velocity above 1 km/s, since the higher impact velocity provides high impact pressure. Also the phase composition of ZnS changed from cubic (zinc blende) to hexagonal (wurtzite) structure. Figure 6-7 represents the TEM images of the ZnMgS powder after the shock wave compression at the impact velocity of 1 km/s. From the TEM image, we can see that the particles of the sample were significantly deformed by the shock wave. The crystallographic defects (stacking faults) were created in some particles as shown in the bottom of Fig. 6-7.

Figure 6-8 shows the photoluminescence spectra of ZnS sample doped with copper

and ZnMgS sample doped with copper. Doping of ZnS with copper showed the blue-green luminescence (Fig. 6-8a) and doping with Mg and Cu resulted in blue-violet luminescence (Fig. 6-8b). This indicates that the shock compression can effectively be applied for increasing the photoluminescence property of ZnMgS b creating crystal defects and doping with other metals.

The shock wave compression of the ZnMgS induced the change of the zinc blend structure ZnS into the wurtzite type ZnS. Also, the shock compression created the stacking faults in the sample. This resulted in the improvement of the photoluminescence and shifting the emission wavelength to the UV spectral range. Since the UV light emitting diodes are demanded for the industrial applications, shock wave treated ZnMgS can be an excellent candidate.

6.4 Conclusions

A new simple catalyst-free low-temperature method for the synthesis of the wurtzite structure ZnS was presented. This is the first method for the ZnS synthesis by the electric discharge. Impulse plasma between two zinc electrodes in the sulfur melt resulted in formation of ZnS. Also the metallic particles of zinc were revealed in the sample. Changing one of the electrodes to magnesium leads to the formation of MgS additionally to ZnS and Zn nanoparticles. During the formation of the ZnS nanoparticles, impulse plasma created crystal defects such as stacking faults, which improve the photoluminescence. In addition, by this method we can combine several processes (synthesis, creating crystal defects, doping, etc) into one.

Shock wave compression of ZnMgS powder was performed. Under the impact velocities of 0.91 km/s and 1.0 km/s, the powder was successfully compacted. Shock wave compression of ZnMgS powder resulted in the phase transformation of ZnS from zinc blend to wurtzite structure. Also shock compression of ZnMgS induced the formation of crystallographic defects, which improved the photoluminescence of the sample by shifting the luminescence from blue-green to blue-violet.

Comparing to ZnMgS sample treated by the shock compression, ZnS nanopowder produced by the impulse plasma in liquid method showed larger number of crystal defects. In addition, nanometer size of the ZnS particles and the wurtzite type structure are

considered as the main advantages.

Since the difficulty of the scaling up and processing of ZnMgS by shock compression method make the industrial application problematic, the wurtzite ZnS nanopowder prepared by the impulse plasma in liquid method was suggested for the industrial application.

References

[1] Gutowski, J., et al. Physica Status Solidi B-Basic Research, 2002. 234(1): p. 70-83

[2] Ray, B. 1 ed. International series of monographs in the science of the solid state, ed. B.R. Pamplin. Vol. 2. 1969, Oxford, London, U.K.: Pergamon Press. 268

[3] Jiang, X., et al. Chemistry of Materials, 2001. 13(4): p. 1213-1218

[4] Yamaga, S., A. Yoshikawa, and H. Kasai. Journal of Crystal Growth, 1988. 86(1-4): p. 252-256

[5] Elidrissi, B., et al. Materials Chemistry and Physics, 2001. 68(1-3): p. 175-179

[6] Ma, C., et al. Advanced Materials, 2003. 15: p. 228-231

[7] Moore, D., et al. Chemical Physics Letters, 2004. 385: p. 8-11

[8] Moore, D., Y. Ding, and Z.L. Wang. Journal of the American Chemical Society, 2004. 126: p. 14372-14373

[9] Moore, D., Y. Ding, and Z.L. Wang. 2006, Georgia Institute of Technology

[10] Li, Y.Q., et al.. Applied Physics Letters, 2006. 88: p. 013115

[11] Zapien, J.A., et al. Applied Physics Letters, 2004. 84(7): p. 1189-1191

[12] Jiang, Y., et al. Journal of Physical Chemistry B, 2004. 108(9): p. 2784-2787

[13] Lefebvre, P., et al. Physical Review B, 1996. 53(23): p. 15440-15442

[14] Wang, Y.W., et al. Chemical Physics Letters, 2002. 357(3-4): p. 314-318

[15] H. Zhang, S.Y. Zhang, M. Zuo, G.P. Li, J.G. Hou, Eur. J. Inorg. Chem. 2005 (2005) 47

[16] X.F. Duan, C.M. Lieber, Adv. Mater. 12 (2000) 298

[17] Q.H. Xiong, G. Chen, J.D. Acord, X. Liu, J.J. Zengel, H.R. Gutierrez, J.M. Redwing, L.C. Lew, Y. Voon, B. Lassen, P.C. Eklund, Nano Lett. 4 (2004) 1663

[18] X.M. Meng, J. Liu, Y. Jiang, W.W. Chen, C.S. Lee, I. Bello, S.T. Lee, Chem. Phys. Lett. 382 (2003) 434

[19] Y.C. Zhu, Y. Bando, D.F. Xue, D. Golberg, Adv. Mater. 16 (2004) 831

[20] S. Kar, S. Chaudhuri, J. Phys. Chem., B 109 (2005) 3298

[21] A. B. Sawaoka, Shock Wave in Materials Science, Published by Springer-Verlag, (1993)

[22] E. Omurzak, M. Matsuda, H. Ihara, T. Mashimo, S. Sulaimankulova. Adv. Mater. Res. 15-17 (2007), 549

[23] T. Mashimo, S. Ozaki, K. Nagayarna. Rev. Sci. Instrurn. 55, 226 (1984)

Table 6-1. Experimental condition for the shock compression of ZnMgS

No.	Weight	Impact velocity	Capsule type	Impact plate	Pressure
1.	1.8 g	0.68 km/s	SS41 12 mm inner diameter	W (1.0 mm thickness)	17.0 GPa
2.	1.8 g	1.0 km/s	SS41 12 mm inner diameter	Cu (2.0 mm thickness)	19.4 GPa
3.	1.8 g	0.91 km/s	SS41 12 mm inner diameter	W (2.0 mm thickness)	23.7 GPa
4.	1.0 g	1.21 km/s	SS41 8 mm inner diameter	W (1.0 mm thickness)	33.3 GPa

a)

b)

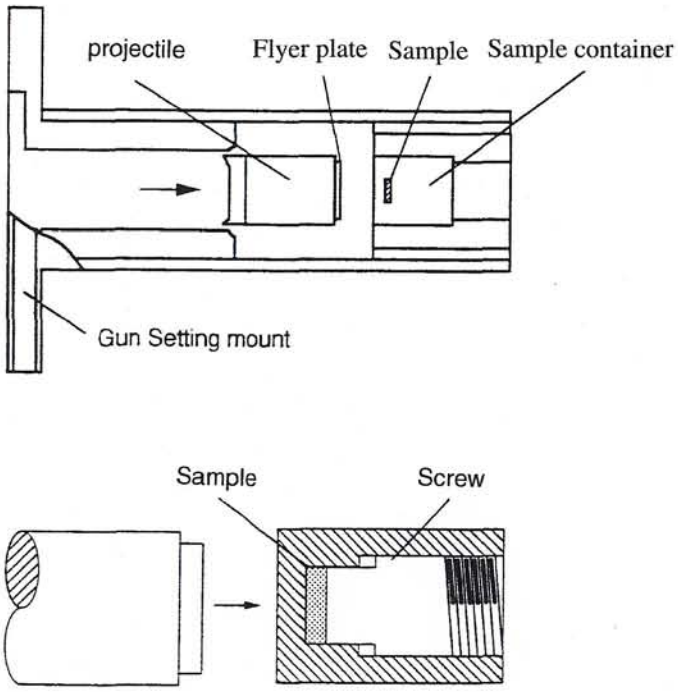

Figure 6-1. a) Photograph of the powder gun used for the shock wave compaction and b) schematic diagram of the powder gun compaction and the cross-section of the sample container capsule

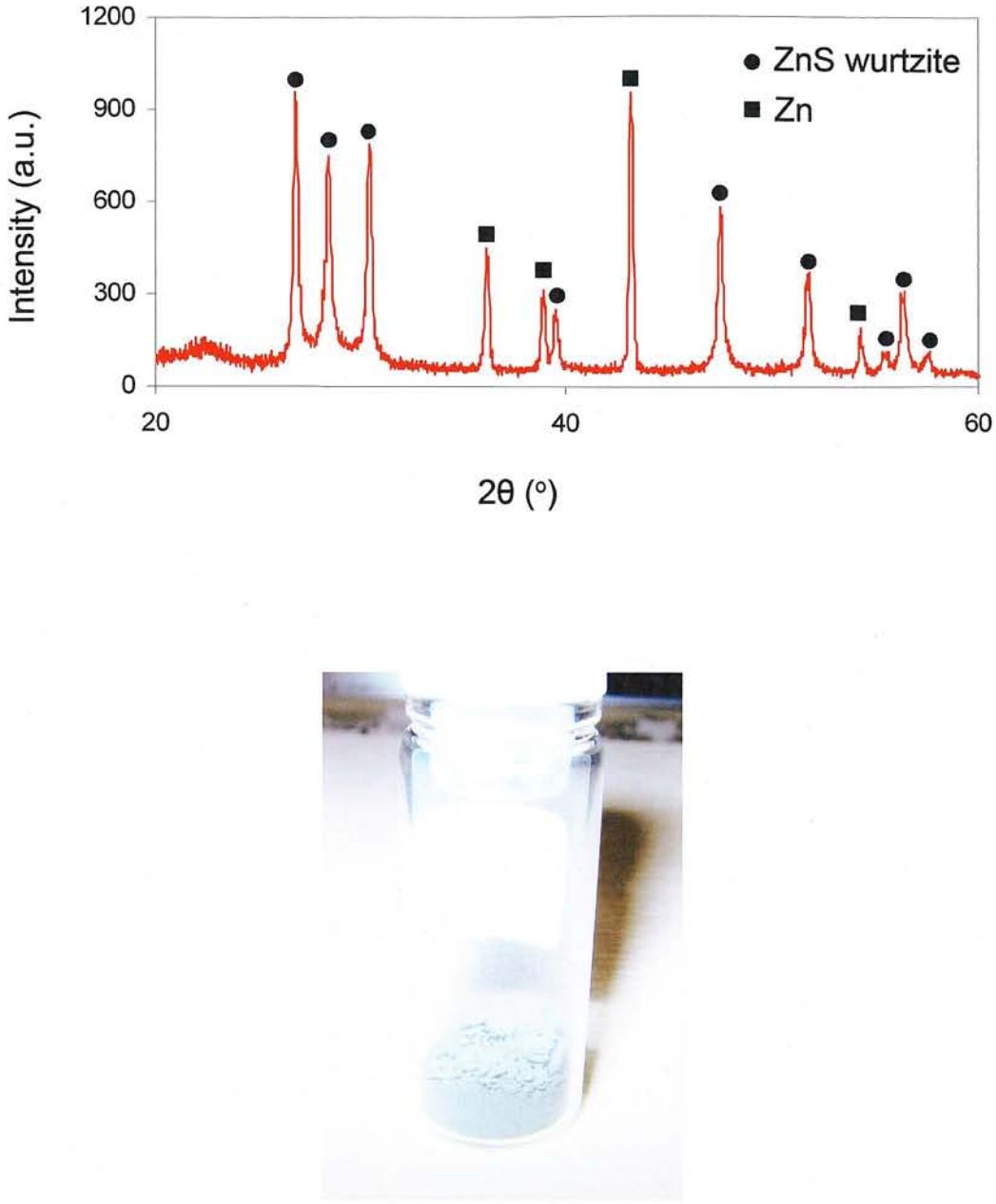

Figure 6-2. XRD patterns of the product of zinc electrodes destruction by impulse plasma in sulfur and a photograph of the sample

a)

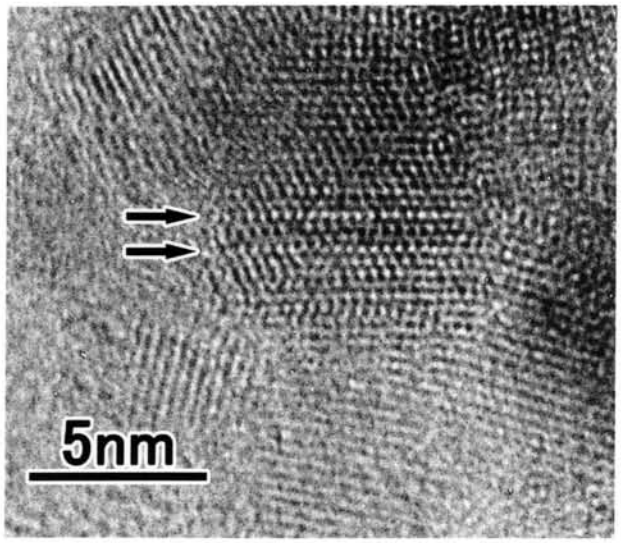

b)

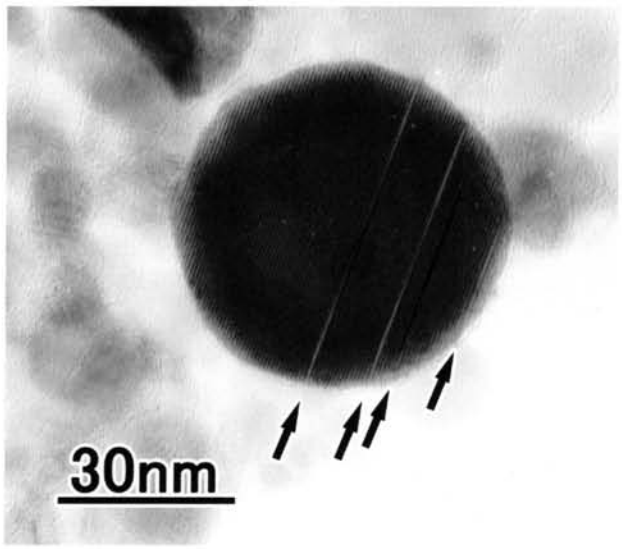

Figure 6-3. a) Lattice image of ZnS particle, produced by the impulse plasma between two zinc electrodes submerged in sulfur, with the stacking faults denoted by arrows and b) HRTEM image of a bigger ZnS particle, produced by the impulse plasma, with the stacking faults denoted by arrows

a)

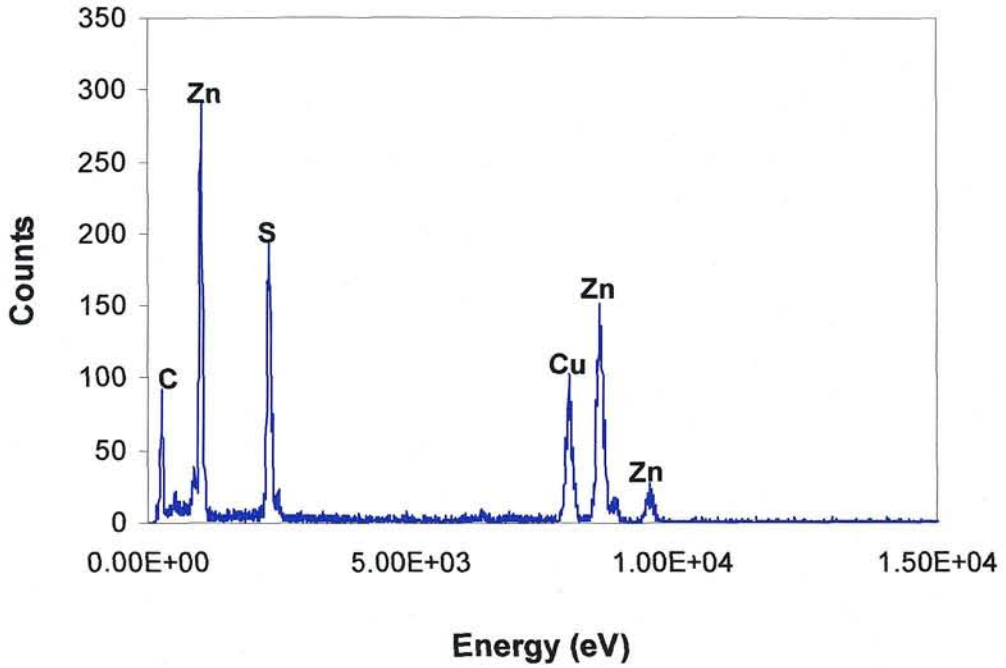

b)

Quantification Results

Element	Weight %	Atomic %	Detector Uncertainty %	Correction	k-Factor
C(K)	19.528	50.553	0.898	0.173	6.279
O(K)	1.284	2.496	0.128	0.514	1.980
S(K)	**18.193**	**17.644**	0.310	0.911	1.101
Cu(K)	21.769	10.652	0.411	0.997	1.757
Zn(K)	**39.223**	**18.653**	0.571	0.997	1.851

Figure 6-4. a) HRTEM EDX spectrum of the particle with the stacking faults shown in the Fig.6-3 and b) the quantification of the peaks indicating that the particle is ZnS

a)

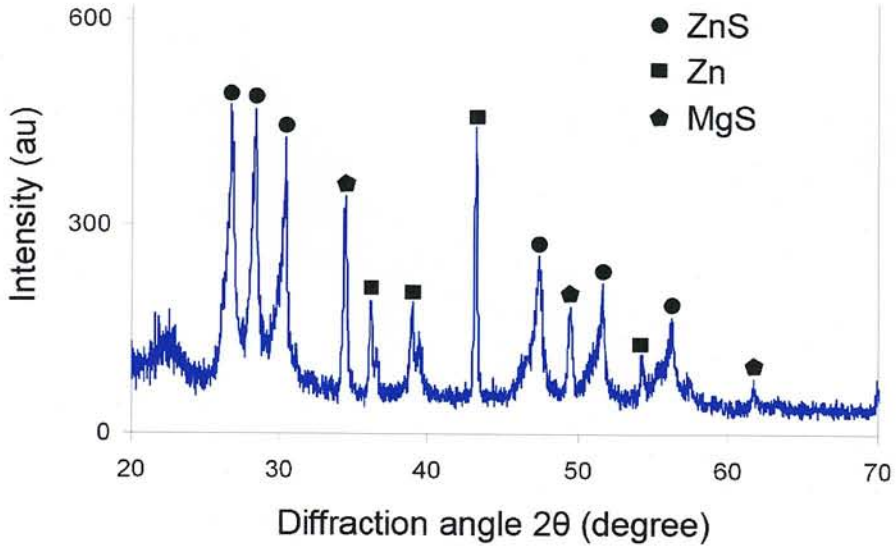

b)

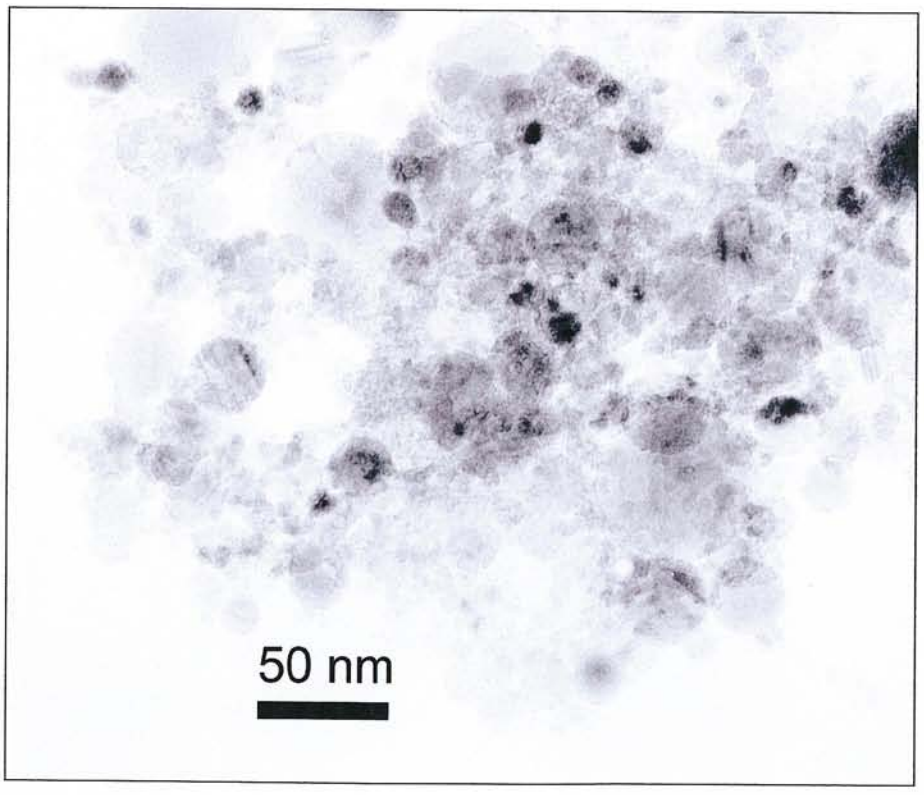

Figure 6-5. a) XRD patterns of the sample produced by the impulse plasma between zinc and magnesium electrodes in sulfur and b) TEM image of this sample

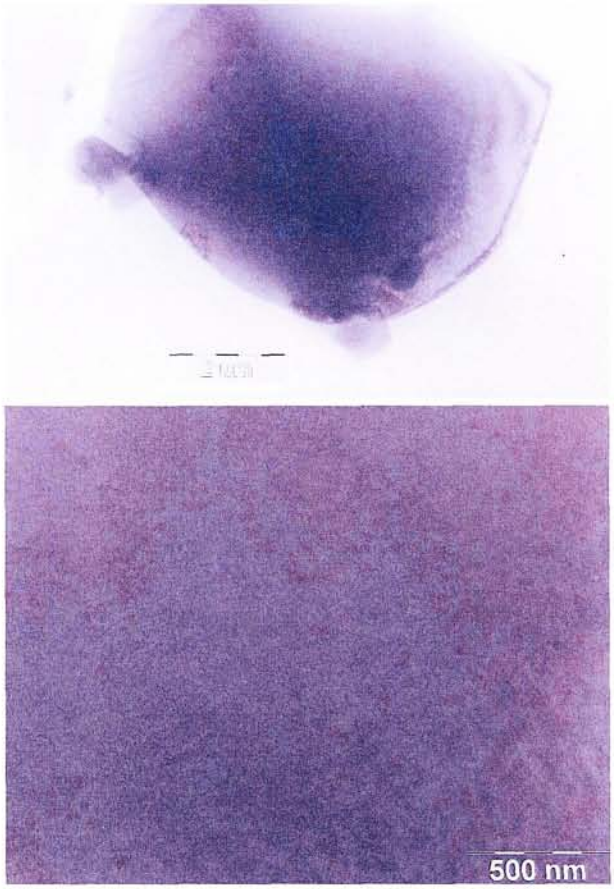

Figure 6-6. TEM images of ZnMgS particle before the shock compression

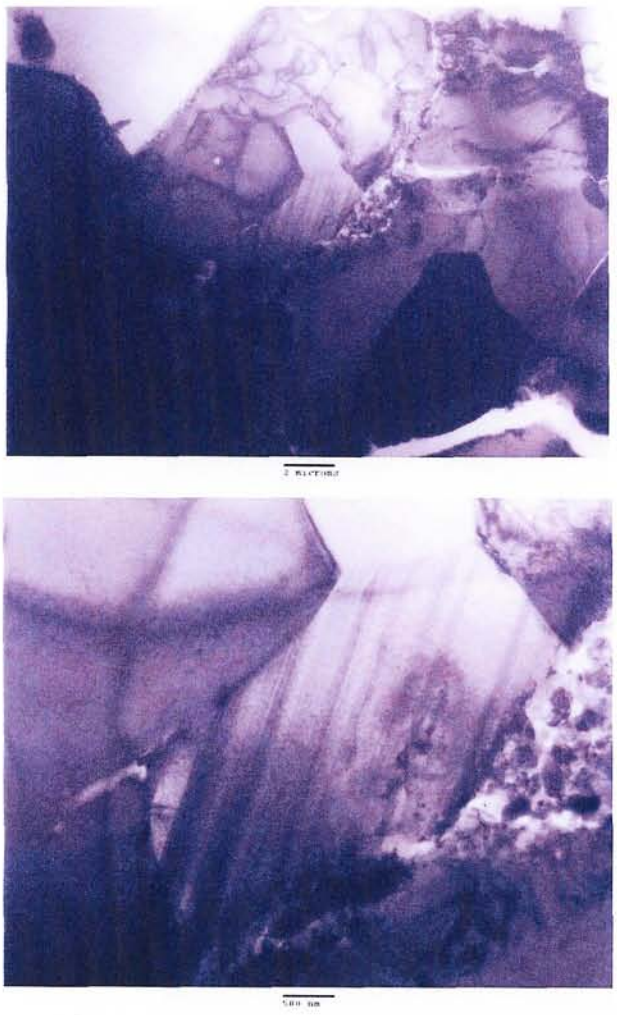

Figure 6-7. TEM images of the stacking faults in ZnMgS crystals, created after the shock loading at 1.0 km/s

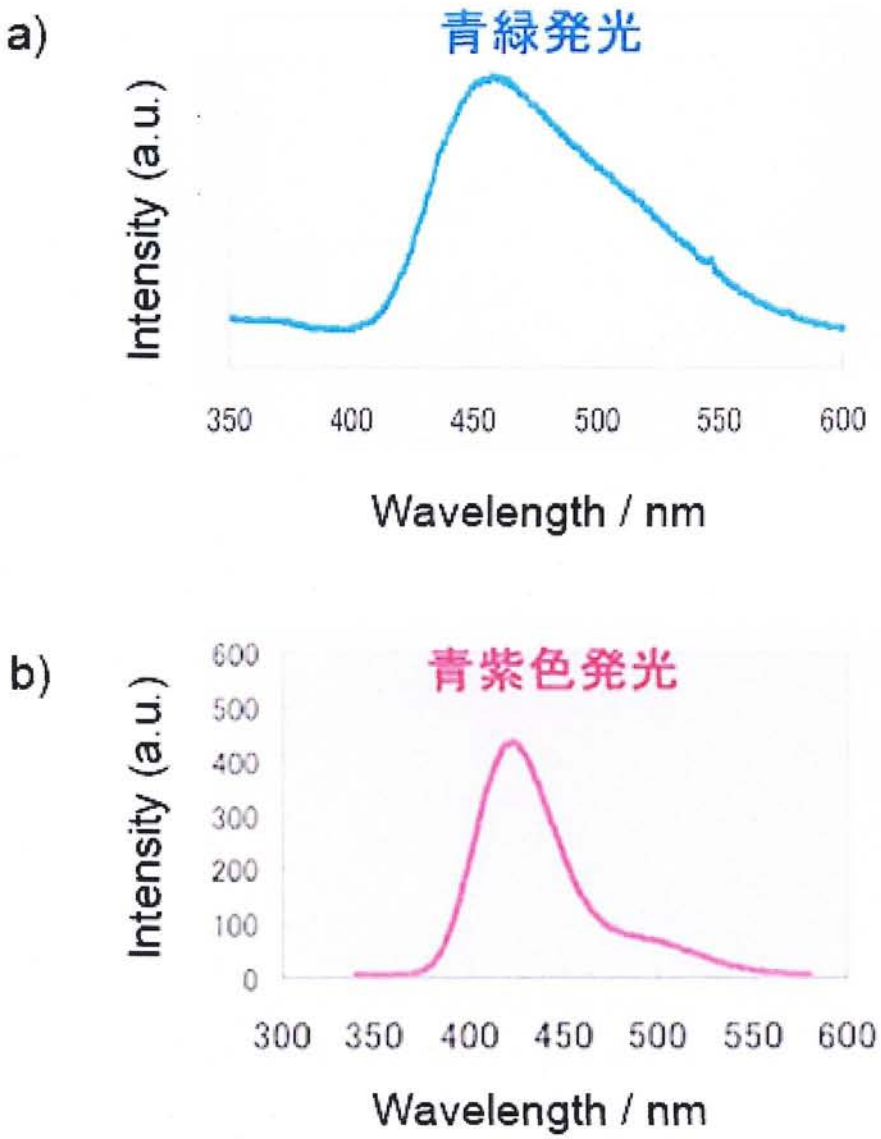

Figure 6-8. a) Photoluminescence spectrum of ZnS:Cu, Cl and b) photoluminescence spectrum of ZnMgS:Cu

Chapter 7
General conclusions

The purpose of this study was the synthesis of nanomaterials by using the impulse plasma in liquid and their characteristics. We have studied the formation of carbon nanostructures, metallic nanoparticles, oxide and sulfide nanoparticles by the impulse plasma in liquid method by using the different combinations of electrodes, different discharge solutions and various experimental parameters such as frequency, impulse energy, etc.

In this dissertation, we presented a new synthesis method for nanomaterials by using the impulse plasma in liquid created by the low voltage spark discharge in dielectric liquid. The new apparatus of this method was produced and installed at the Kumamoto University for the research of this subject. The study of the synthesis of the fullerene C_{60}, nanoparticles of Cu, Yb, TiO_2 and ZnS nanoparticles were performed. Brief conclusions on each chapter are given below.

In the *Chapter 1*, current state of the nanomaterials sciences, background of this research and the purpose and novelty of this study was described. Nanoscience and nanotechnology are considered as the most promising fields of science that are expected to make future scientific and technological breakthroughs. Many scientists, including leaders of science and technology, Nobel laureates are themselves amazed that the emerging nanotechnology may provide humanity with unprecedented control over the material world. Synthesis of nanomaterials and understanding the formation mechanisms in order to precisely produce the desired structures and materials will undoubtedly contribute to the nanoscience and nanotechnology.

Even though a huge number of researches have been conducted in the area of the nanomaterials research, the fundamental questions of the nanomaterials formation mechanism poorly understood. In addition, despite the large number of synthesis techniques for the nanomaterials synthesis, high quality samples with higher performance and low cost is still challenging.

The impulse plasma in liquid by the low voltage spark discharge in dielectric liquid has every condition for formation of nanomaterials of any metal, oxides, sulfides, compounds, etc. It is a very simple method with a number of advantages for the synthesis of nanomaterials of various materials. Therefore, the purpose of this study was to develop a new method for the nanomaterials synthesis using the impulse plasma in liquid and their characteristics by the state-of-the-art research equipment available.

In the *Chapter 2*, the description of the new synthesis method for the nanomaterials by the impulse plasma in liquid was given. A new apparatus of the impulse plasma in liquid method apparatus was successfully produced and installed at the Kumamoto University. In the design of the circuit, priority was given to the electrical and health safety. All parts of the circuit were purchased separately and assembled in a 600x500x250 mm sized metal case manually by ourselves. Power for the device is supplied by inverter with adjustable frequency between 1-1500 Hz, voltage of 50-200 V, and current up to 20 A. The discharge current and voltage waveforms were measured by the digital oscilloscope. The duration of a single impulse was measured to be 10 μs. Impulse plasma device can generate impulse of 10 μs duration with up to 100 mJ.

In the *Chapter 3*, we presented a new synthesis method for the copper and ytterbium nanoparticles by using the impulse plasma in liquid. Copper nanoparticles prepared by this method were smaller than those by arc method by a factor of >5. The present method can be used for the synthesis of various kinds of metal and compound nanomaterials.

The mechanism of the nanoparticles formation by the impulse plasma in liquid was proposed. The temperature of the hot plasma produced by the impulse plasma is same with the arc plasma, however, due to fast quenching and short duration of pulses, temperature increase in the impulse plasma in liquid has very sharp peak and does not expand to the surrounding medium. So the temperature of the liquid remain the same with the room temperature, while in the water arc it increases up to the boiling point of water and even more.

In the *Chapter 4*, a new method for synthesis of fullerene C_{60} by using the impulse plasma in liquid was described. The fullerene C_{60} was for the first time synthesized by electric discharge in liquid between two graphite electrodes submerged into toluene. The purity of the synthesized fullerene C_{60} was >99 %. This method does not need vacuum system, cooling system, etc., in addition to the low electrical power. The phase composition of the sample produced at the different frequency remained the same, however,

increasing the frequency of the impulse plasma resulted in the increasing the formation of the small sized particles.

In the *Chapter 5*, the blue colored amorphous TiO_2 nanopowder was synthesized using impulse plasma in liquid method. HRTEM analysis showed that the blue amorphous TiO_2 consists of the anatase crystals with less than 10 nm size. This sample was stable up to the temperature of 400 ℃. By increasing the temperature of water, the crystallinity of the blue sample increased. The blue TiO_2 obtained by this method showed higher absorbance in the visible light than the commercial photocatalyst ST-01. It is expected that this sample exhibits excellent photoluminescence and catalytic properties under the visible light. The experiments on the photocatalytic property of the blue amorphous TiO_2 under the UV light showed that the annealed at 400 ℃ blue amorphous TiO_2 sample has high photocatalytic property than the commercial anatase photocatalyst.

In the *Chapter 6*, the synthesis of the wurtzite type ZnS nanoparticles was reported for the first time by the electric discharge method. Impulse plasma between two zinc electrodes in sulfur resulted in formation of ZnS. Also the metallic particles of zinc were revealed in the sample. By replacing one of the electrodes by magnesium rod electrode, we synthesized MgS additionally to ZnS and Zn nanoparticles. Large numbers of stacking faults, which improve the photoluminescence property, were observed in both ZnS and ZnS/MgS nanocrystals. It was suggested that ZnS nanoparticles by the impulse plasma in liquid show excellent photoluminescence properties without any additional treatment.

TEM analysis of the sample treated by the shock wave at the impact velocity of 0.68 km/s did not show any significant change of the crystal state. However, powders treated by the shock wave with the impact velocity at 1.0 km/s and 0.91 km/s were successfully compacted and were hard enough. Shock compression of ZnMgS induced the phase transition of ZnS from zinc blend to wurtzite structure. Also, the crystallographic defects were created in some ZnMgS particles by the shock loading. This resulted in the improvement of the photoluminescence and shifting the emission wavelength (from 460 nm to 430 nm) to the direction of UV spectral range.

Acknowledgements

First, I would like to thank those who had a direct impact on my scholastic studies.

I have very much gratitude to my supervisor Prof. T. Mashimo for his kind guidance, generous support and encouragements consistently in carrying out of this doctoral dissertation. My gratitude is also to my committee members: Prof. Y. Matsumoto, Prof. H. Akiyama, Prof. Y. Kawamura, Prof. A. Yoshiasa, Prof. J. Watanabe.

Also, I am grateful to my teacher Prof. S. Sulaimankulova from the Laboratory of Nanotechnology, Institute of Chemistry and Chemical Technology, National Academy of Sciences, Kyrgyzstan, for her kind advises and encouragements for accomplishment of this study and also I thank the members of the laboratory Mr. J. Jasnakunov, Ms. N. Mairykova, Ms. J. Shyityeva for their support and encouragement.

I am grateful to Prof. H. Ihara, Dr. A. Shundo, Mr. H. Nomoto from the Faculty of Engineering of the Kumamoto University for their support in HPLC, DLS, etc analysis. I would like also thank to Prof. M. Nishida, Prof. Iwamoto, Dr. M. Matsuda of the Faculty of Engineering of the Kumamoto University for their kind help and discussions on the TEM and HRTEM analysis. My thanks also to Prof. Y. Matsumoto, Dr. S. Ida, Dr. U. Unal of the Faculty of Engineering of the Kumamoto University for their help and discussions in measurements of photocatalytic property of samples. Also I thank to Prof. H. Yokoi, Mr. H. Momota of the Faculty of Engineering of the Kumamoto University for their help in measurement of Raman spectra of samples.

Also I am grateful to Mr. Y. Uemura and Mr. N. Kawayanagi for their help as my tutors with life in Japan. I would like also thank Dr. X. Huang, Dr. T. Kinoshita, Dr. X. Fan, Dr. Y. Zhang, Mr. Y. Uemura, Mr. S. Inoue graduated students from Mashimo laboratory for their support, discussions and encouragements.

I also would like to thank my colleagues Mr. Y. Iguchi, Ms. R. Bagum, Mr. T. Inoue, Mr. N. Kawayanagi in Mashimo Laboratory for their helpful experimental supports in the accomplishment of this work.

This work was supported by the 21st Century Center of Excellence Program of the Kumamoto University on the Pulsed Power Science and Its Applications.

Main papers of the present study

Chapter 2

1. E. Omurzak, J. Jasnakunov, N. Mairykova, A. Abdykerimova, A. Maatkasymova, S. Sulaimankulova, M. Matsuda, M. Nishida, H. Ihara, T. Mashimo; Synthesis method of nanomaterials by pulsed plasma in liquid Journal of Nanoscience and Nanotechnology 2007, 7, pp. 3157-3159
2. U.A. Asanov, J.K. Jasnakunov, E. Omurzak, S.K. Sulaimankulova; Nanomaterials from the impulse plasma in liquid Selected works of the National Academy of Sciences of the Kyrgyz Republic (50th anniversary issue), Bishkek, Ilim, 2004, pp.21-31

Chapter 3

1. J. Jasnakunov, E. Omurzak, SK. Sulaimankulova, U.A. Asanov; Nanomaterials from Impulse Plasma in Liquid Izvestia VUZov, Bishkek, V.8, 2004, pp.11-14

Chapter 4

1. E. Omurzak, J. Jasnakunov, N. Mairykova, A. Abdykerimova, A. Maatkasymova, S. Sulaimankulova, M. Matsuda, M. Nishida, H. Ihara, T. Mashimo; Synthesis method of nanomaterials by pulsed plasma in liquid Journal of Nanoscience and Nanotechnology 2007, 7, pp. 3157-3159
2. E. Omurzak, M. Matsuda, H. Ihara, T. Mashimo, S. Sulaimankulova; Preparation of nanocrystalline inorganic materials by impulse plasma in liquid Advanced Materials Research 2006, 15-17, pp. 549-552
3. U.A. Asanov, S.K. Sulaimankulova, J.K. Jasnakunov, E. Omurzak; Phase composition of graphite destruction in Impulse Plasma in Liquid Chemical Journal of Kazakhstan, 2004, pp. 144-148

Awards related to this work

"The Best Poster Presentation Award" at the 2nd KITECH-KU Symposium on Bulk Metallic Glasses and Pulsed-Power Processing, Aso, Japan, January 20-21, 2005

"Silver Award" at the 4th International COE Forum on Pulsed Power Science, Aso, Japan, 5-6 September, 2007